ISSN 2708-6437(Online)
2708-6429(Print)

Journal of Engineering Advancements

Editor-in-Chief:
Prof. Dr. Mohammad Mashud

Volume 01 Issue 03

SciEn

Published by:
SciEn Publishing Group

Journal of Engineering Advancements
Apt. # 6 C-D, House # 191
Road # 9/A, Dhanmondi R/A
Dhaka-1209, Bangladesh
Email: jea@scienpg.com Website: www.scienpg.com/jea/

Published in: October 2020
Published by: SciEnPG

Price: Each Issue BDT 200.00 (US$ 15) **ISSN:** 2708-6437 (Online) 2708-6429 (Print)

Journal of Engineering Advancements

Published by: SciEn Publishing Group

Apt. # 6 C-D, House # 191, Road # 9/A
Dhanmondi, Dhaka-1209, Bangladesh
Email Address: jea@scienpg.com

www.scienpg.com/jea/

This page is intentionally left blank

Journal of Engineering Advancements

Volume 01, Issue 03 October 2020

CONTENTS

Original Articles

This page is intentionally left blank.

SciEn
Journal of Engineering Advancements Vol. 01(03) 2020, pp 70-75 https://doi.org/10.38032/jea.2020.03.001

Post-consumer PET Bottle Recycling: Chemical Dose Optimization

*Md. Shahadat Hossain** *and Md Anisur Rahman*

Department of Chemical Engineering and Polymer Science, Shahjalal University of Science and Technology, Sylhet - 3114, Bangladesh

Received: August 17, 2020, Revised: September 11, 2020, Accepted: September 12, 2020, Available Online: September 15, 2020

ABSTRACT

Polyethylene terephthalate (PET) bottles are being used in our daily life and consequently go to the landfills after their use. Additionally, virgin PET resins are produced from nonrenewable resources, such as fossil fuels, whose reserves are depleting continuously. Therefore, to maintain ecological and environmental balances as well as for sustainable development, post-consumer PET (pcrPET) bottles should be recycled. Among many recycling processes, mechanical recycling of pcrPET is attractive due to lower cost involvement. One of the most crucial and important processes of mechanical recycling is hot washing for contaminants removal. Hot washing uses a cleaning solution made of caustic soda (NaOH) and detergent at elevated temperature. In this paper, caustic soda and FORYL LFO (FLO) detergent doses were changed gradually to investigate effective contaminants removal through colorimetric study. Finally, concentration vs. absorbance graphs from colorimetric study suggests that 2% NaOH and 2% FLO detergent is the optimum chemical dose at hot washing for pcrPET recycling.

Keywords: PET Bottle; Recycling; Chemical Dose; NaOH; Detergent; Colorimetric Analysis.

1. Introduction

Plastic bottles are widely used at beverage, water, oil, and pharmaceutical industries in Bangladesh [1], [2]. Most of them are directly goes to the landfill after their first hand use but those bottles are not biodegradable [3]. As a result, they create potential hazard for our agricultural lands, sewage systems as well as for water networks across the country [4]. On the contrary, Bangladesh is currently producing different plastic products from both imported virgin polymer and locally recycled plastics [3], [5]. Bangladesh used 75,000 metric tons (MT) plastic raw materials mainly for packaging materials, household accessories and producing construction materials in 2015 [5], [6]. At the same time, Bangladesh recycled around 65 percent of its post consumer plastic materials and this trend was increasing in every year [2], [6]. This post consumer plastic recycling provides Bangladesh two fold advantages: firstly for plastic waste management and secondly for saving money which otherwise would have been used for importing virgin polymer [4], [6],[7]. Unfortunately, up to now most of the recycled plastic materials are used only by small and medium-sized enterprises (SMEs) and yet no big plastic conglomerates have used recycled plastic materials due to its inferior quality [5]. In a book, United Nations ESCAP [6] showed that SMEs used 60 percent of the total recycled plastic materials and subsequently produced low quality plastic products. Rest of the unused and recycled plastic materials was exported to China. For instance, Bangladesh exported USD 6 million worth recycled plastic materials between July 2008 and January 2010 due to lack of proper recycling technology [5], [6]. However, Bangladesh has huge demand for quality recycled plastic materials inside the country [2]. Therefore, recycled plastic materials quality should be improved through proper plastic collection method and proper washing for decontamination.

Among various plastic materials, most widely used plastics in Bangladesh are polyethylene (PE), polyvinylchloride (PVC), polypropylene (PP), polyethylene terephthalate (PET) and polystyrene (PS) [2], [3]. Among which post consumer PET (pcrPET) is recycled mostly and has been used by SMEs for bottle production for beverage, oil, water, and medicine industry as well as for PET sheet and polyester fiber production. But still now pcrPET is recycled in Bangladesh by conventional method where it is manually sorted firstly, later grounded and finally cold washed by detergent and subsequently dried for decontamination. But, this conventional recycling method produces inferior quality recycled PET flakes in Bangladesh.

However, it is widely known that during pcrPET materials recycling, caustic soda (NaOH) and detergent are used in hot washing, but dosage of chemicals is different in different countries [8]-[10]. This is because pcrPET bottles are collected in wide variety of methods in different counties, which make them contain different amounts of dirt and contaminants [11]-[13]. On the basis of contaminants adherence to pcrPET bottles after their first hand use, 1–3 % NaOH along with small amount of detergent are used for contaminants removal [8], [10]. Some authors also report usage of antifoaming agent in hot washing for foaming phenomena reduction [8]. Therefore, if pcrPET bottles are recycled in Bangladesh, chemical dosage in hot washing should be determined by considering amount and types of contaminants present in those post consumer bottles [14], [15]. If improper amount of washing chemicals are used in hot washing step of recycling, it will give yellowish color in subsequent recycling steps, for example, extrusion, injection molding, and blow molding due to presence of trace amount of NaOH in recycled PET materials [13], [16]-[19]. Therefore, determination of chemical dosage in hot washing is crucial for total pcrPET bottle recycling. Use of proper chemical dosage will

*Corresponding Author Email Address: shahadat06-cep@sust.edu

turn potential environmental hazard into valuable PET flakes and subsequently will reduce the environmental pollution through PET bottles recycling. In this paper, pcrPET bottles generated across the country were collected and then a step by step recycling process was developed for contaminants removal by employing chemical dosage. Different chemical dose – varying proportion of NaOH and FORYL LFO (FLO) detergent – were tested in hot washing, a crucial step of recycling process, to find out the optimum chemical dose for pcrPET bottles recycling.

2. Methodology

2.1 Experimental Set-up

It was assumed in this study that a pcrPET recycling plant is running with a production capacity of 1.0 MT recycled PET flakes per hour where 30 minutes of hot washing for pcrPET flakes is employed. A hot washer (is shown in Fig. 1) with a 100 rpm stirrer uses 6 m^3 water and NaOH plus FLO detergent dose for pcrPET flakes hot washing. Therefore, it is estimated that every 30 minutes hot washer contains 0.50 MT flakes within 6 m^3 of water for hot washing. However, this paper used small scale hot washer accommodating 1 liter (L) water for 30 minutes of hot washing. Consequently, 0.083 kg pcrPET flakes were used for hot washing with NaOH and FLO detergent dosage at elevated temperature.

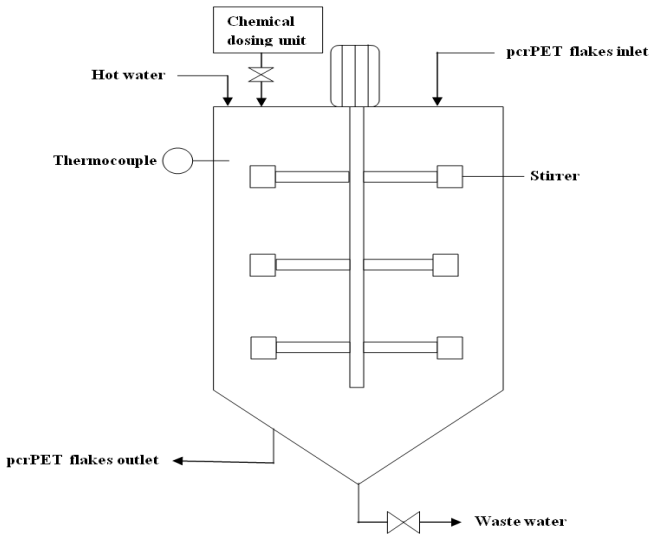

Fig. 1 Schematic of a hot washer.

2.2 Sample Collection

pcrPET bottles sample was collected from five big suppliers who collected bottles through their small collection hub across the country and 2 kg sample was collected from each supplier. Moreover, another 2 kg pcrPET bottles sample was collected directly from waste collection bins and landfills. Later, all the samples, i.e., 12 kg bottles were mixed together to homogenize pcrPET bottles generated throughout the country. However, each time 0.1 kg pcrPET bottles were taken from homogenized sample for subsequent sample pretreatment.

2.3 Sample Pretreatment

pcrPET bottles taken from homogenized sample also contained other plastics such polyethylene (PE), polypropylene (PP), polyvinyl chloride (PVC) etc. and metals alongside pcrPET due to lack of proper post consumer plastic waste collection method in Bangladesh. The undesired plastics were removed manually in this step.

2.4 Cold Washing

After initial pretreatment, pcrPET sample were washed with cold water at ambient condition to remove dirt from the sample in a rector called cold washer. Cold washer was mainly a 2 L bucket containing a slow speed stirrer (50 rpm) which accommodated initially taken pcrPET sample. Cold washing provided relatively clean pcrPET bottles which later chipped into desired size in subsequent processing steps.

2.5 Sample Cutting

Cleaned PET bottles sample were chipped into 7-13 mm sized pcrPET flakes (Fig. 2) in accordance with the recycled PET flakes size of several large recycled PET flakes manufacturer from Asia to Europe [20]-[22]. Sample cutting was carried out without any kind of drying.

Fig. 2 pcrPET flakes sample for hot washing after cutting into desired 7 – 13 mm size.

2.6 Gravity Separation

Gravity separation in another water reactor was employed to separate PE, PP, PVC etc. materials from pcrPET flakes which finally provided flakes sample for hot washing. This flakes sample contained mostly glue and dirt contaminants which were removed in hot washing.

2.7 Hot Washing

Hot washing used NaOH and FLO detergent dose at 80 °C to remove contaminants from pcrPET sample flakes while lower and higher temperature was avoided due to ineffective washing and excessive foaming correspondingly. Hot washing was carried out in small scale reactor which has 30 minutes residence time for sample flakes. Moreover, this small reactor also contained a high speed stirrer (100 rpm) for effective contact between flakes and hot washing chemicals. Chemical dose - NaOH and FLO detergent percentage - was changed gradually in both reactors until hot washing produced contaminants free quality recycled PET flakes.

Actually, NaOH and FLO detergent dose percentages were employed as hot washer reactive volume (1 L). For example, detergent dose was slowly augmented from 1% to 3% percent of total hot washer volume (1 L) but NaOH dose was constant. Three different constant NaOH dose values such as 1, 2 and 3% were selected. Each time different detergent dose, varying from 1% to 3%, at a constant NaOH dose was used in hot washing. Then optimum chemical dose in hot washing reactor at 80 °C temperature was determined from recycled PET flakes colorimetric analysis.

2.8 Sample PET Flakes Washing and Drying

After hot washing and before characterization by colorimetric analysis, recycled PET flakes were washed vigorously and dried. This is because the presence of trace amount of unused hot washing chemicals (NaOH and FLO detergent) can produce yellowish color in recycled PET flakes. Therefore, extensive cold washing, for example, centrifugal washing, float washing and spray washing were carried out one after another for at least 10 minutes to remove unused hot washing chemicals. After hot washing chemicals removal, PET flakes were dried for 10 minutes at 130 °C for water removal. Drying of PET flakes produced contaminants free, dry and quality recycled PET flakes which were again dried at 220 °C for another half an hour.

2.9 Recycled PET Flakes Colorimetric Analysis

After consecutive dryings, recycled PET flakes from every chemical dose were stored individually. Stored recycled flakes from every single dose were used to prepare pcrPET solution with 0.025, 0.05, 0.1, 0.15, and 0.2 concentrations. Then a colorimeter was used for absorbance measurement against every concentration. Concentration vs. absorbance curve for different chemical doses were compared with pcrPET (without using any chemical dose) and pure PET to find out optimum chemical dose at hot washing. Before that two calibration curves, one for pure PET and another one for pcrPET with any chemical dose, were prepared for aforementioned comparative study.

3. Results and Discussion

3.1 Calibration Curve of Pure PET and pcrPET

Colorimeter absorbance was measured against different pure PET concentrations and results are represented in Fig. 3. Pure PET means those PET that have not used in any packaging or other applications. It is observed that absorbance is gradually increasing with the increment of PET concentrations. Results of absorbance at different concentrations of pcrPET are also shown in the same figure. Similar trend was observed in this case as like as that obtained in case of pure PET. However, higher absorbance value is achieved in case of pcrPET than pure PET as expected. Higher absorbance value is resulted from higher contaminations adherence after pcrPET bottles first hand use. Furthermore, every concentration of both types of PET is also compared. It was observed that for every single concentration, pure PET's absorbance is lower than that of pcrPET. This scenario was obtained since pure PET had no chance to adhere any kind of contaminations such as dirt, glue, PVC etc. as compared to pcrPET.

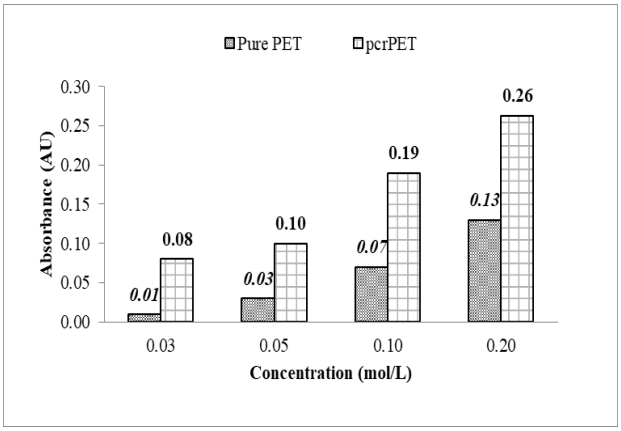

Fig. 3 Comparison of colorimeter absorbance between pure and pcrPET.

3.2 Hot Washing with Varying Chemical Dose

3.2.1 Hot washing with 1% NaOH and 1%, 2%, and 3% FLO (detergent)

Initially, PET flakes hot washing started with lower NaOH dose, 1%, but detergent dose was increased gradually from 1% to 3%. Among them lowest chemical dose, 1% NaOH and 1% detergent, produced blackish recycled PET flakes (Fig. 4 a) after consequent drying at 130 °C and 220 °C. NaOH used in the hot washing acted as aggressive cleaning agent for pcrPET flakes surface but such a lower dose – 1% NaOH – could not remove mainly the dirt and glue contaminants from the flakes [8], [23]. As a result, discoloration of recycled PET flakes happened after consecutive drying since glue and dirt were identified as contaminants responsible for flakes discoloration by several authors [8], [24] However, blackish color from dirt contaminants offsets the slight yellowish color resulted from glue contaminants; resulted blackish recycled PET flakes at lower chemical dose [25]. Overall, as the lowest chemical dose did not remove contaminants such as dirt, glue etc. properly, colorimeter analysis of recycled PET flakes was not performed at this chemical dose.

Later, hot washing chemical dose was increased further to 1% NaOH and 2% FLO level. Recycled PET flakes produced through this chemical dose are presented in Fig. 4 b whereas its colorimetric analysis is shown in Fig. 5. In Fig. 5, a comparative analysis between this recycled flakes with pure and pcrPET is drawn. Graphical representation at Fig. 5 shows that recycled flakes with this chemical dose stays in between the pure and pcrPET flakes. Actually, 1% NaOH and 2% detergent dose (1% vs 2%) lowered the absorbance of recycled flakes highest 57.89% (at 0.01 mol/L) compared to pcrPET and on average this chemical dose lowered 40.25% absorbance. This implies that above chemical dose can significantly remove contaminations from pcrPET.

On the contrary, still there is a chance to improve contaminants removal as recycled PET flakes line stays above the pure PET line as shown in Fig. 5. Therefore, chemical dose again increased at 1% NaOH and 3% FLO level. Although recycled flakes of this chemical dose were cleared satisfactorily, heavy foaming problem was encountered during PET flakes hot washing with this chemical dose. Therefore,

colorimetric analysis was skipped for this chemical dose too since commercial application of this chemical dose is impractical due to heavy foaming at hot washing reactor.

(a)

(b)

Fig. 4 Recycled PET flakes after hot washing and drying with (a) 1% NaOH and 1% detergent (b) 1% NaOH and 2% detergent.

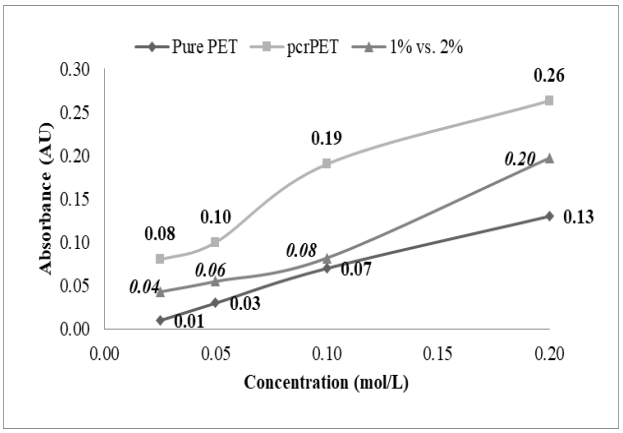

Fig. 5 Colorimetric analysis of recycled PET flakes with 1% NaOH and 2% percent FLO dose and comparative study between recycled and pure and pcrPET.

3.2.2 Hot washing with 2% NaOH and 1%, 2%, and 3% FLO (detergent)

As Fig. 5 suggests that further improvement is possible for contaminants removal, chemical dose was changed, especially, NaOH dose was increased to 2% and FLO dose was remained same as previous 1%, 2% and 3%. However, lowest chemical dose in this combination again produced blackish recycled PET flakes and therefore colorimetric analysis was excluded for this dose.

Then subsequent chemical dose combination, 2% NaOH and 2% FLO, produced comparatively cleaner recycled PET flakes and their colorimetric representation is shown in Fig. 6 (2% vs. 2%). Fig. 6 shows that highest 62.5% absorbance reduction (at 0.05 mol/L concentration) is possible for recycled PET flakes with 2% NaOH and 2% FLO dose and on average 50.29% absorbance reduction is possible compared to pcrPET. This means that contaminants removal has been improved further due to chemical dose increase. As a result, recycled flakes line approaches further closer to pure PET line and away from pcrPET line in Fig. 6.

However, 2% NaOH and 3% FLO produces slightly yellowish recycled PET flakes instead of white and cleaned flakes after drying at 130 °C and 220 °C. Moreover, huge foaming problem was also faced with this chemical dosage. Naturally detergents are prone to foam formation but in this chemical dose heavy foaming was formed due to addition of higher proportion of detergent to the very close to bubbling point of water during hot washing. Simultaneously large percentage of detergent and proximity of hot washing temperature (80 °C) to bubbling point of water were responsible for heavy foaming [18], [26]. Due to above mentioned problems, commercial application of this chemical dose for pcrPET recycling is not suggested and the colorimetric analysis of this recycled PET is thus excluded.

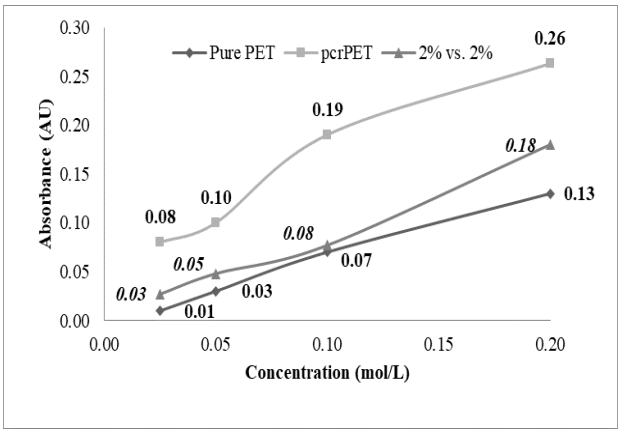

Fig. 6 Colorimetric analysis of recycled PET flakes with 2% NaOH and 2% percent FLO dose and comparative study between recycled and pure and pcrPET.

3.2.3 Hot washing with 3% NaOH and 1%, 2%, and 3% FLO (detergent)

Previous hot washings were carried out at a constant NaOH dose either at 1% or 2% and varying percentages of FLO dose such 1%, 2% and 3%. From previous result it was found that blackish recycled flakes were produced at lower chemical

dose (1% FLO) and foaming problem was encountered at higher chemical dose (3% FLO). As a result, above two chemical doses were excluded while NaOH dose was increased further to 3%.

However, 3% NaOH and 2% percent FLO detergent produces recycled PET flakes which turned completely yellowish after subsequent drying at previously mentioned temperatures. This indicates that the extra addition of chemical during hot washing was not removed in several washing steps. As a result, remaining NaOH on PET flakes surface turned yellowish after successive drying at 130 °C and 220 °C. This yellowish phenomenon can also be explained by natural tendency of NaOH; turns yellowish after drying at elevated temperature [10], [19]. In addition, higher usage of NaOH incurs higher operating cost to PET recycling. As this chemical dose produces undesired recycled PET flakes, colorimetric analysis of this dosage has not also been included in this paper.

3.3 Hot washing chemical dose optimization

Recycled PET flakes produced through two best chemical doses (1% NaOH and 2% FLO, 2% NaOH and 2% FLO) at hot washing are compared together with pure and pcrPET in Fig. 7 to find out optimum chemical dose for hot washing. It can be observed that the absorbance of recycled flakes were always lower at every concentration compared to that of pcrPET. This means that the above two chemical doses are capable of removing attached contaminants from pcrPET. However, 2% NaOH and 2% FLO dose has lower absorbance value than other chemical dose which implies that this chemical dose has higher efficiency for contaminants removal from pcrPET at every concentration. Moreover, the absorbance of recycled PET flakes corresponding to this chemical dose has closest proximity to pure PET, which clearly indicates that recycled PET flakes produced through this dose is closest to pure PET- in terms of quality-than other recycled PET flakes. Therefore, 2% NaOH and 2% FLO detergent dose is the best suited candidate for pcrPET flakes hot washing.

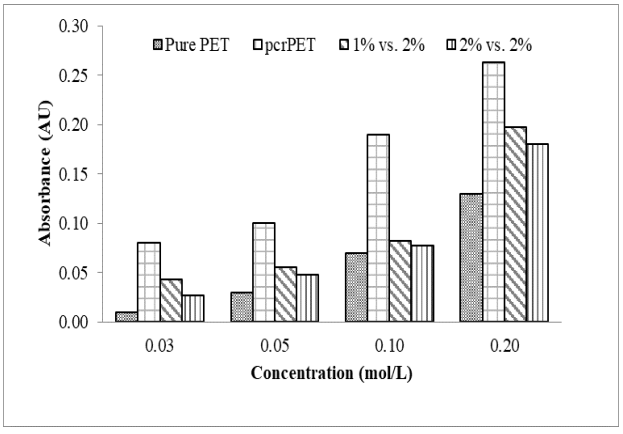

Fig. 7 Comparative study between pure and pcrPET with recycled PET at two chemical doses.

4. Conclusion

Mechanical recycling is an attractive process across the world for pcrPET bottles recycling due to its lower capital and operating cost involvement. Successful recycling mainly depends of contaminants removal from post consumer bottles after their first time use. This study used hot washing for effective contaminants removal. For hot washing, NaOH and detergent FLO was used in different proportions. Lower detergent dose, for example, 1% FLO, could not remove the dirt contaminants properly from the pcrPET resulted blackish recycled PET flakes. On the contrary, higher detergent dose – 3% FLO – created heavy foaming during the hot washing which made difficult to finish the hot washing and subsequent collection of recycled PET flakes for further colorimetric analysis. Similarly, higher NaOH dose such as 3% NaOH produced yellowish recycled PET flakes (undesired quality) after hot washing and further drying. It occurred due to the presence of higher amount of NaOH at PET flakes surface after hot washing and later extensive cold washing. Finally, 1% NaOH and 2% detergent dose and 2% NaOH and 2% detergent dose produced desired quality recycled PET flakes. Among them 2% NaOH and 2% FLO detergent (a non ionic detergent) was found to be optimum chemical dose for hot washing since this chemical dose removed the highest percentage of contaminants from pcrPET. However, this paper studies only chemical dose optimization at the hot washing, but there are several other factors that should be considered for complete mechanical recycling of post consumer PET bottles.

Acknowledgement

This research was funded by ***SUST Research Centre*** in the year of 2017 -18.

References

[1] Bari, Q.H., Hassan, K.M. and Haque, M.E., 2012. Solid waste recycling in Rajshahi city of Bangladesh. *Waste management*, *32*(11), pp.2029-2036.

[2] Matter, A., Ahsan, M., Marbach, M. and Zurbrügg, C., 2015. Impacts of policy and market incentives for solid waste recycling in Dhaka, Bangladesh. *Waste Management*, *39*, pp.321-328.

[3] Mourshed, M., Masud, M.H., Rashid, F. and Joardder, M.U.H., 2017. Towards the effective plastic waste management in Bangladesh: a review. *Environmental Science and Pollution Research*, *24*(35), pp.27021-27046.

[4] Rahman, S.M., Shams, S. and Mahmud, K., 2010. Study of solid waste management and its impact on climate change: a case study of Dhaka City in Bangladesh. In *Proceedings of International Conference on Environmental Aspects of Bangladesh (ICEAB), September 4, 2010, University of Kitakyushu, Kitakyushu, Japan* (pp. 229-231).

[5] Hasan, M.M., <IDLC Monthly Business Review - May 2015 .pdf>, in: C.R.M. Industry & Equity Analysis Team, IDLC Finance Limited (Ed.) MONTHLY BUSINESS REVIEW, IDLC Finance Limited, Dhaka 1212, 2015, pp. 2-15.

[6] U. Nations, U.N. Economic, S.C.f. Asia, t.P. Trade, I. Division, Enabling Environment for the Successful Integration of Small and Medium-sized Enterprises in

Global Value Chains: Country Studies of Bangladesh, Nepal and Sri Lanka, United Nations ESCAP2012.

[7] Afroz, R., Hanaki, K. and Tudin, R., 2011. Factors affecting waste generation: a study in a waste management program in Dhaka City, Bangladesh. *Environmental monitoring and assessment*, *179*(1-4), pp.509-519.

[8] Awaja, F. and Pavel, D., 2005. Recycling of PET. *European Polymer Journal*, *41*(7), pp.1453-1477.

[9] Karayannidis, G.P., Nikolaidis, A.K., Sideridou, I.D., Bikiaris, D.N. and Achilias, D.S., 2006. Chemical recycling of PET by glycolysis: polymerization and characterization of the dimethacrylated glycolysate. *Macromolecular Materials and Engineering*, *291*(11), pp.1338-1347.

[10] Malik, N., Kumar, P., Shrivastava, S. and Ghosh, S.B., 2017. An overview on PET waste recycling for application in packaging. *International Journal of Plastics Technology*, *21*(1), pp.1-24.

[11] Nikles, D.E. and Farahat, M.S., 2005. New motivation for the depolymerization products derived from poly (ethylene terephthalate)(PET) waste: A review. *Macromolecular Materials and Engineering*, *290*(1), pp.13-30.

[12] T.W.M. Organization, Best Practices in PET Recycling Clear PET, Clean Flake Specifications for Fiber, Bottles, Film and Sheet, Strapping, Engineered Resins, and Depolymerization, 1998.

[13] Park, S.H. and Kim, S.H., 2014. Poly (ethylene terephthalate) recycling for high value added textiles. *Fashion and Textiles*, *1*(1), pp.1-17.

[14] Welle, F., 2011. Twenty years of PET bottle to bottle recycling—an overview. *Resources, Conservation and Recycling*, *55*(11), pp.865-875.

[15] Yousuf, T.B. and Rahman, M., 2007. Monitoring quantity and characteristics of municipal solid waste in Dhaka City. *Environmental monitoring and assessment*, *135*(1-3), pp.3-11.

[16] Sinha, V., Patel, M.R. and Patel, J.V., 2010. PET waste management by chemical recycling: a review. *Journal of Polymers and the Environment*, *18*(1), pp.8-25.

[17] Romão, W., Franco, M.F., Bueno, M.I.M. and De Paoli, M.A., 2010. Distinguishing between virgin and post-consumption bottle-grade poly (ethylene terephthalate) using thermal properties. *Polymer testing*, *29*(7), pp.879-885.

[18] Mancini, S.D., Schwartzman, J.A.S., Nogueira, A.R., Kagohara, D.A. and Zanin, M., 2010. Additional steps in mechanical recyling of PET. *Journal of Cleaner Production*, *18*(1), pp.92-100.

[19] Koo, H.J., Chang, G.S., Kim, S.H., Hahm, W.G. and Park, S.Y., 2013. Effects of recycling processes on physical, mechanical and degradation properties of PET yarns. *Fibers and Polymers*, *14*(12), pp.2083-2087.

[20] E.-. recycling, Technical specifications: pet flakes – quality specification, Poland, 2020. https://ergis-recycling.eu/en/content/PET-Polyethylene-terephthalate/technical-specifications [Accessed 06 September 2012]

[21] M.R. Technology, PET Specification: Clear PET flakes, United Kingdom, 2020. http://marsrecyclingtechnology.co.uk/home/pet-specification/ [Accessed 06 September 2012]

[22] G.I. Limited, PET Bottle Flakes: Recycled PET Flakes, India, 2020. https://www.gravitaindia.com/pet-bottle-flakes/ [Accessed 06 September 2012]

[23] Welle, F., 2016. Investigation into cross-contamination during cleaning efficiency testing in PET recycling. *Resources, Conservation and Recycling*, *112*, pp.65-72.

[24] Welle, F., 2011. Twenty years of PET bottle to bottle recycling—an overview. *Resources, Conservation and Recycling*, *55*(11), pp.865-875.

[25] Zhu, B., Liu, J., Pan, R., Wang, S. and Gao, W., 2015. Fabric seam detection based on wavelet transform and CIELAB color space: A comparison. *Optik*, *126*(24), pp.5650-5655.

[26] Hossain, M.S. and Mozumder, S.I., 2018. Post consumer polyethylene terephthalate (PET) recycling in bangladesh through optimization of hot washing parameters. *American Scientific Research Journal for Engineering, Technology, and Sciences (ASRJETS)*, *40*(1), pp.62-76.

SciEn
Journal of Engineering Advancements Vol. 01(03) 2020, pp 76-84 https://doi.org/10.38032/jea.2020.03.002

Finding the Reasons for the Delay Time in a Highway by Analyzing the Travel Time, Delay Time and Traffic Flow Data

T M Junaid Bashar, Md. Sabbir Hossain and Shah Istiaque*

Department of Urban and Regional Planning, Khulna University of Engineering & Technology, Khulna-9203, Bangladesh

Received: August 27, 2020, Revised: September 28, 2020, Accepted: September 29, 2020, Available Online: October 03, 2020

ABSTRACT

The objectives of this study are to show a comparison among travel time, running time, delay in peak and off-peak hours on different days of a week, and reasons behind the delay time. Moving car observer method has been carried out to count the traffic flow, journey time, running time, and delay time. Total vehicle flow, and comparative vehicle flow during the peak hour and off-peak hour for workdays and weekend days were surveyed to show a relationship between delay time and traffic flow. As the traffic flow increases the delay time also will increase. To measure the reasons behind the delay time of Fulbarigate-Daulatpur road, spot speed study was done in two intersections of the road. The 15th percentile speed for Religate intersection road is 10 K.P.H. That means 85% of vehicles tends to go faster than 10 K.P.H. in this section. And hence vehicles with less than or equal 10 K.P.H. are responsible for increasing the delay time in this area. This speed limit should be prohibited in this section to reduce delay time and congestion. For the Mohosin More road intersection, the prohibited speed is also 10 K.P.H. Easy bike and Mahindra account for the congestion of these intersections and tend to stop in these intersections to collect passengers which creates unwanted queue in this study area. Controlling traffic flow at intersections can be a possible way to reduce the congestion rate of Fulbarigate-Daulatpur road.

Keywords: Spot Speed; Journey Time; Travel Time; Percentile; Congestion; Delay Time.

1. Introduction

The provision of adequate and equitable service for all groups is the main target of urban planning. Transportation is one of the most important elements of such a service [1]. Transportation is a process that involves the movement of commuters, goods, and services from a given point of origin to a specific destination [2]. It determines the regional patterns of development, economic viability, environmental impacts, and maintenance of socially acceptable levels of quality of life. It is a means to access business activities, education, employment, and recreational opportunities [3]. Various transportation modes are available like road-based, railway based, air-based, and water-based [4]. In our country, road-based transportation is dominant among them. In a road-based transportation system, the public transport system is most popular [5].

"Since the end of the Second World War, high demand for mobility increases due to rapid urbanization and economic growth in third world cities" [6]. Like other developing countries in Bangladesh, problems related to the lack of traffic mobility are getting extremely high [7]. Bangladesh cannot bear the cost of the financial and ecological misfortune that came about because of this serious traffic obstacle [8]. Main urban areas like Dhaka (eats up to 3.2 million working hours/day), Chittagong, and Khulna are under the disturbing worry of this issue [9]. Khulna, the third biggest city of Bangladesh, in such a case is close to repeating a similar incidence [10].

In respect of Khulna division's transportation system, Khulna-Jessore Highway is the most important road network for both intra and intercity connectivity. "Besides after the completion of Padma Bridge transportation between the Khulna region and the Dhaka region will become even easier which will increase the economic activities of Khulna. To support this economic growth and future public demand a well-planned transportation system is a prerequisite" [11]. The common modes of public transportation in Khulna are pedal rickshaw, baby taxi, battery bike and auto-rickshaws etc. [12].

However, a comparison among travel time, running time, delay in peak, and off-peak hours on different days of a week is shown in this study, and the reasons behind the delay time are found out. Several traffic studies e.g. volume study, speed study, etc. have been carried out for this study. By conducting travel time, speed, and delay studies congestion can be measured [13]. Moving car observer method is used in measuring travel time, delay time, vehicle flow. Delay can be measured by doing field measurement, simulation, analytical derivation, or by using a combination of these methods [14]. The reasons behind the delay time at two intersections of Fulbarigate-Daulatpur road is carried out by using spot speed. This type of evaluation of the public transport system is very suitable for a highly populated country like Bangladesh [15]. As the western part of Khulna is facing acute traffic congestion due to the haphazard movement of traffic, the amount of delay time has increased. Particularly the delay time at major intersections and road sections in Khulna Metropolitan City is increasing faster [16]. A huge number of slow-moving vehicles create a huge delay time due to the lack of proper management [7].

There are 66 National highway routes in Bangladesh and 9 of them are from Khulna division. The route chosen for this research is called Khulna-Jessore road and our study area Fulbarigate to Daulatpur is within Khulna City Corporation. The road covers 3.2 kilometers distance [17]. Thus, this research will assist to develop a proper transportation system. In the end, the output of this research can be useful in further tasks associated with the Khulna-Jessore highway.

*Corresponding Author Email Address: junaidbashar@gmail.com Published by: SciEn Publishing Group

2. Methodology

To conduct the study, traffic flow, travel time, running time, and spot speed are studied. The study has been conducted based on primary data. Primary data sources are - Reconnaissance survey, Spot Speed Survey, Running Speed, Journey Speed Study, and Delay Studies. Moving car observer method has been used for the measurements of running speed and journey speed. Congestion and delay time in two intersections of Fulbarigate-Daulatpur road is carried out by using spot speed. Spot speed has been surveyed through a direct-timing procedure.

2.1 The moving car observer method

The field survey was carried out to collect the data on Fulbarigate to Daulatpur which has a 3.9 km length. To count the traffic flow, average journey Speed, average running speed, and delay time, moving car observer method has been used. Several test runs are made along the road section and a group of observers records various parameters. Four observers were fixed for recording four types of data. The four types of data were –

- Total journey time, delay points and delay time
- Number of overtaking vehicles
- Number of overtaken vehicles
- Number of modes coming from the opposite direction

The average journey time (min.) for all vehicles in a traffic stream in the direction of flow (q) is given by following equation.

$$q = (M_a+M_w)/(T_a+T_w)$$

$$T_{avg}=T_a-(M_w/q)$$

Where, T_{avg} = Average journey time, Tw = Average journey time when vehicle is travelling in the stream,

M_w = Overtaking vehicle minus Overtaken vehicle, M_a = Average number of vehicle in opposite direction,

Ta = Average journey time when vehicle is travelling in opposite stream [18].

2.2 Spot speed study

For our study area, the stopwatch method is preferred. For calculating spot speed 60/100 m length at each link of a highway will be taken which has free flow. When the vehicles passed at the first reference point, the first observer signaled the second observer and then the second observer started the stopwatch, and finally when the vehicles crossed the other reference points, then stop the watch and recorded the time. The speed of a particular vehicle will be calculated from how much time it takes to cross a certain distance. Thus, from known distance and time, found out the vehicle's spot speed. The spot speed of the vehicles was measured four times in two days.

The cumulative speed distribution curve was prepared to analyze the spot speed condition for different speed percentile groups. The 15th, 50th, 85^{th,} and 98th percentile speeds are four parameters that are commonly used in traffic safety and traffic engineering. For example, the 15th percentile speed reflects the minimum or critical speed limits, 50th percentile speed reflects median speed limit, 85th percentile speed reflects the optimum speed limit and 98th percentile speed reflects the maximum or design speed limit [19], [20].

Table 1 Moving car observer data collection sample.

Morning Weekend Peak Hour						
Location	Direction	Journey Time (minutes)	Stop Time (minutes)	Number of Vehicles		
				Over Taking	Over Taken	In Opposite Direction
Fulbarigate to Daulatpur	N-S	6.7	0.6	51	47	159
		5.8	0.3	63	37	127
		6.8	0.5	55	51	161
		6	0.4	57	42	147
		5.6	0.2	68	39	138
		6.9	0.35	52	49	162
Total		37.8	2.35	336	265	894
Mean		6.3	0.4	56	44.2	149

Source: Field Survey

3. Data collection & calculation

As shown in Table 1 data collection sample and sample calculation of moving car observer Survey. Same procedure carried out both workdays and weekends during Peak Hours (8.00-9.00 AM, 12.00-1.00 PM, 5.00-6.00 PM) and Off-Peak Hours (10.00-11.00 AM, 3.00-4.00 PM) in both directions.

4. Data Analysis

For finding out the possible causes of delay time and the level of service of the Fulbari to Daulatpur highway- this study focused on several factors. First of all, through the vehicle flow survey the amount of total vehicle flow during the peak hour and off-peak hour for workdays and weekend days were determined to find out if there was any anomaly in total vehicle flow number in this road. Secondly using the spot speed survey in different intersections in the road the minimum and maximum speed for different types of vehicles available was found out. After analyzing the data the ideal speed for every vehicle has been determined. It also shows those vehicles which travel below the 15th percentile speed that causes unwanted congestion in that road. Here, to visualize the data of spot- the related speed map for the two different intersections is also prepared. Through this analysis, the connection between vehicle flow and vehicle speed is figured out which eventually leads to those factors which impact the delay time in this road.

Table 2 Sample calculation of moving observer survey.

Calculation	
M_w = Overtaking vehicle minus overtaken vehicle	11.8
M_a = Average number of vehicle in opposite direction	149
Tw = Avg. journey time when vehicle is travelling in the stream	6.3 min
Ta = Avg. journey time when vehicle is travelling in opposite stream	6.4 min
(Flow) Q veh./hr =	759 veh./hr
Avg. Journey time	5.37 min
Avg. journey speed = (3.9*60) / 5.7	43.57 Kmph
Avg. Running time = Avg. journey time – Avg. Stopped Delay	4.98 min.
Avg. Running Speed = (3.9 * 60)/4.98	47 Kmph

4.1 Journey time and delay time study

This study considers more than one intersection to gather data and both of the intersections don't have any traffic signal. That means the delay time found in this study is caused by other factors than by the traffic signals. Here the average journey time, running time, and delay time is calculated for workday and weekend during the pick and off-pick hours. This study considers both sides of the vehicle flow (North to South and South to North) to analyze the travel time and delay time conditions for these intersections.

As Journey time = Running time + Delay time, the journey time is always significantly more than the running time. The more the difference between the journey time and running time the more the delay time is. Now delay time can be caused by many factors including traffic signal, road condition (Ex: Potholes, speed breaker, road width), vehicle type (Ex: Car, Bus, Auto rickshaw, Rickshaw), total number of vehicles, etc. Now this study area doesn't have any traffic signals that means, other factors that cause traffic jams or traffic delays are the reason behind the delay time.

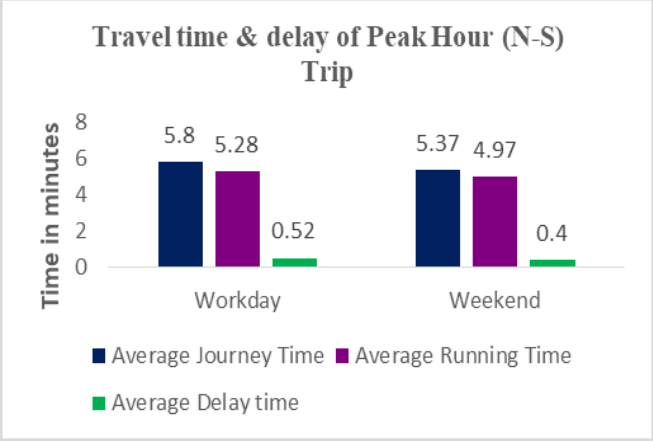

Fig. 1 Travel time & delay of peak hour (N-S) trip.

As shown in Fig. 1 travel time & delay of peak hour (N-S) trip workday has the highest travel time & delay between workday and weekend, same for the return trip (S-N) Peak Hour workday has the highest travel time & delay as shown in Fig. 2, for Travel time & delay of off-peak period (N-S) trip workday has the highest Travel time & delay is shown in Fig. 3, Fig. 4 shows the return of off-peak period trip (S-N).

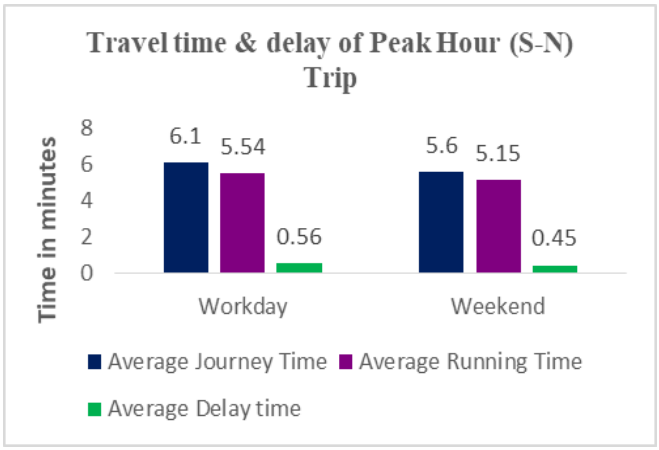

Fig. 2 Travel time & delay of peak hour (S-N) trip.

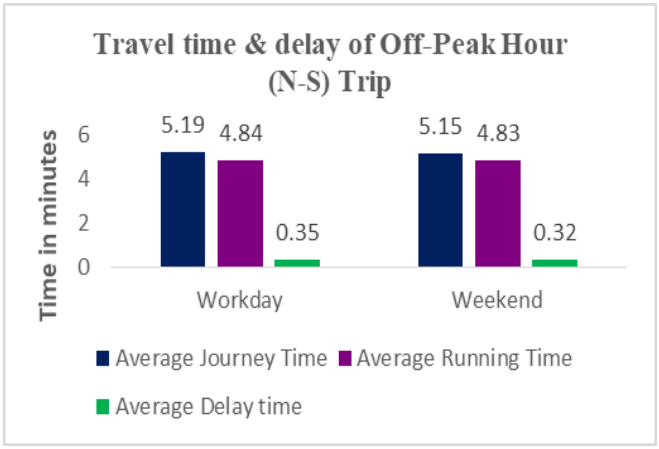

Fig. 3 Travel time & delay of off-peak hour (N-S) trip.

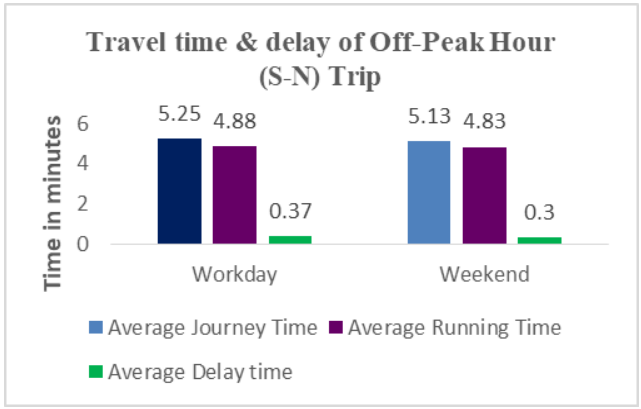

Fig. 4 Travel time & delay of off-peak hour (S-N) trip.

In workdays for the South to North (S-N) trip the average delay time was the maximum (0.56 minutes) during peak hours. And during the off-peak hours of weekend days, the delay time was the minimum (0.30 minutes) for the same South to North (S-N) trip. Even the average delay time (0.40 minutes) during the peak hours in the weekend days (Fig. 1) is greater than the average delay time during the off-peak hours of working days (Fig. 3).

Normally in peak hours, the number of vehicles remains higher than the off-peak hours. So that means the number of

vehicles can be the prominent factor for the increased amount of delay time during the peak hours in the workdays. If the delay time of the study area becomes perfectly equivalent to vehicle flow, then it will mean that the total number of vehicles is the number one factor for delay time in this road. And it will also mean that if the number of vehicles increases every time the delay time also increases in this road too if the other factors remain the same.

4.2 Vehicle flow analysis and related travel time-delay time comparison

To analyze the traffic flow behavior of the study area the vehicle flow chart was prepared. It also explains the possible cause of journey time and delay time differences during peak and off-peak hours for both workdays and weekend days. The comparative vehicle flow for both directions of the road during the peak and off-peak hours in workday and weekend is shown in Fig. 5 and Fig. 6.

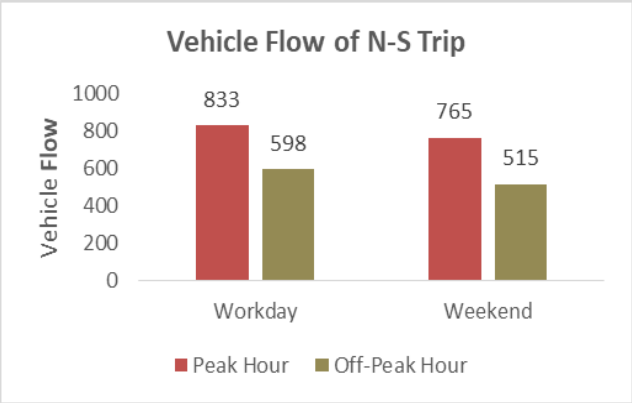

Fig. 5 Vehicle flow of N-S trip.

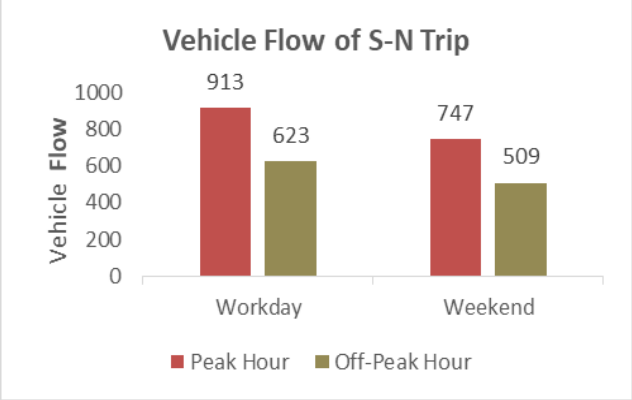

Fig. 6 Vehicle flow of S-N trip.

Workday had the highest Vehicle flow in peak hour for both directions of a vehicle trip. Here, the S-N trip shows a bigger number of vehicle flow in this study area. Most importantly, the total number of vehicles during peak hours of workdays was 833, and 913 which are greater than the off-peak hour's vehicle flow in workdays. These relations remain the same for both North to South (N-S) and South to North (S-N) trips. That means in this study area the total number of vehicles is always higher during the peak hours and hence the traffic pressure also remains higher during the peak hours of both workdays and weekend days and for both side of the trip.

The journey time and delay time data also show the exact fact of increased traffic pressure during the peak hour of both workdays and weekends in both directions of the roads (Fig. 1-4). So in the study area, there is a direct relation of vehicle flow number and the average delay time. According to the data shown in Fig. 1-6, as the total number of vehicles increases in peak hours, the delay time also increases as result.

4.3 Spot speed analysis

Spot speed analysis was performed to determine the speed distribution of different vehicles (Easy bike, Mahindra, Motorcycle, Bus, Truck) available in the traffic stream of this study area. Spot speed frequency distribution curve and cumulative distribution curve have been analyzed for both intersections (Religate and Mohosin More) to find the vehicle types which are directly responsible for the increased delay time in this study area.

4.3.1 For Relegate intersection

The collected speed datasets were grouped into several speed-class interval sections. Within these sections, the number of vehicles was counted to prepare the speed frequency distribution table. From this table, the arithmetical mean speed and a histogram of speed-class intervals against the percentage frequency of vehicle numbers were developed (Fig. 7). Here the speed represents the average speed of all the collected vehicle's speed.

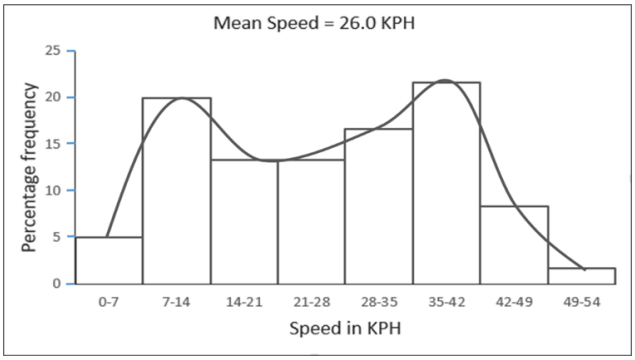

Fig. 7 Spot speed frequency distribution curve for Religate intersection area. (Source: Field Survey)

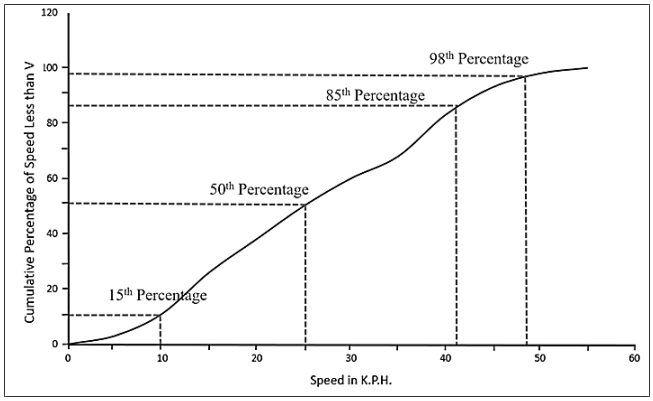

Fig. 8 Cumulative speed distribution curve for Religate intersection road area. (Source: Field Survey)

The average speed of vehicles in the Religate intersection area was 26.0 K.P.H. with a standard deviation of 12.66 which means speed fluctuates a lot during traffic congestion. From Fig. 7 it is clear that the speed of vehicles does not tend to cluster to the mean speed. But the frequency increases if the speed deviates slightly from the mean speed value. This indicates that there are

a significant amount of vehicles travel both at high speed and low speed in this section.

4.3.1.1 Cumulative distribution curve

The cumulative speed distribution curve for the relegate intersection area has been prepared from the speed-class interval and frequency table. To prepare the curve the speed-class intervals are plotted in the X-axis the cumulative percentage of speeds for each class intervals are plotted on the Y-axis. Then from the curve, the related percentile speed is identified (Fig. 8).

The related percentile speed for Fig. 8 are as follows:

i. The 15th percentile speed for Religate intersection road is 10 K.P.H. That means 85% of vehicles tends to go faster than 10 K.P.H. in this section. And hence vehicles with less than or equal 10 K.P.H. are responsible for increasing the delay time and congestion significantly in this area. So the 10 K.P.H speed limit should be prohibited in this section. This will reduce congestion and the unnecessary overtaking tendency of the other drivers in this section.
ii. The 50th percentile speed for this section is 23.6 K.P.H. which the median speed for the observed data set. It represents the average speed of the total traffic stream. It means half of the vehicles travel faster than this 50th percentile speed and half of the vehicles travel slower than this.
iii. The 85th percentile for the Religate intersection is 41.20 K.P.H. which represents that under a free-flowing condition 85% vehicles go in this speed or slower than this. And only 15% of vehicles travel faster than this speed. The 85th percentile speed is commonly used in traffic engineering and traffic safety guidelines as it is considered as the quickest safe speed for any traffic in a road under a free-flowing condition [19].
iv. The 98th percentile speed for the Religate intersection area is 47.50 K.P.H. That means 98% of the vehicles travel equal or less than this speed. This speed is normally considered as the design speed of any road [21].

Table 3 reveals that Mahindra and Easy bike have the highest coefficient of variation with a maximum speed of 30 K.P.H and 23 K.P.H. respectively. It means that they could move faster if they don't face any congestion. Mahindra and Easy bike account for a very large portion of traffic composition on the road. The minimum speed of Mahindra and Easy bike go lower than the 15th percentile speed for this section.

Table 3 Spot Speed statistics of different types of vehicles on Religate intersection.

Vehicle type	Speed of Vehicles				
	Mean	Maximum	Minimum	Standard Deviation	Coefficient of variations
Easy bike	12.31	23.00	4.00	5.95	.48
Mahindra	17.40	30.00	5.75	8.90	.51
Motorcycle	33.33	53.20	12.41	12.41	.37
Private Car	34.35	47.50	15.20	10.21	.30
Bus	32.59	45.60	13.50	9.63	.30
Truck	26.31	43.29	12.50	10.36	.39

It means that if queuing is formed during congestion, this traffic mode makes the congestion more acute as other vehicles need to overtake opportunities while approaching to move. The direct field survey data (Fig. 9) also upholds the results of Table 3. The minimum spot speed of Easy and Mahindra found lower than the 15th percentile speed in this intersection with a speed of only 4 K.P.H and 5.75 K.P.H respectively. According to the field survey data, Easy bike and Mahindra often stops in this intersection to collect passenger which creates an unwanted queue. This consequently results in traffic congestion and travel time delay.

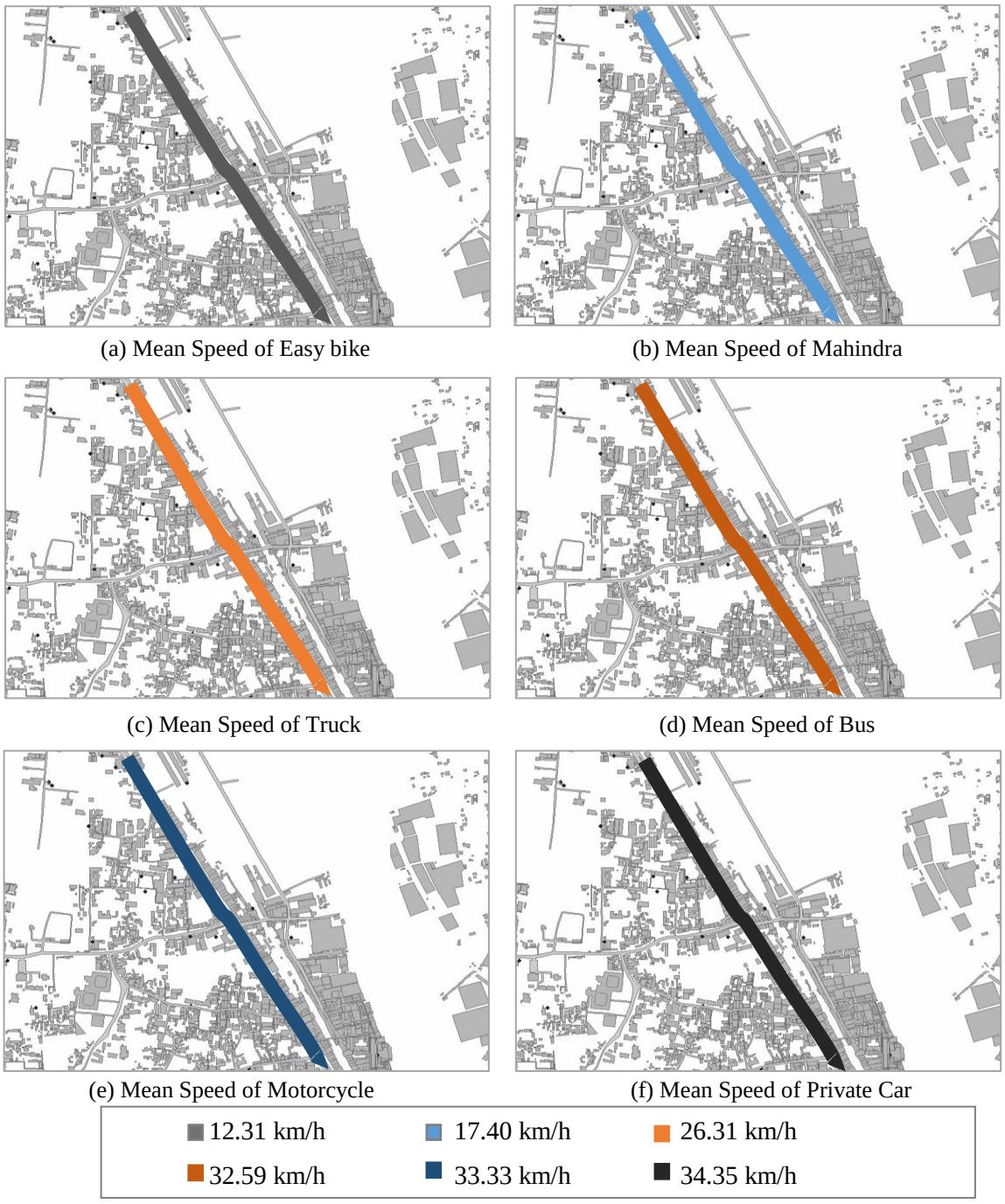

Fig. 9 Mean speed map for different vehicles in the Religate More intersection.

4.3.2 For Mohosin More intersection

The mean speed of Mohosin More intersection was 25.7 K.P.H. with a standard deviation of 12.3. That means most of the speed varies from 13.4 K.P.H to 38 K.P.H. The spot speed frequency distribution curve shows that the speed of vehicles was not also showing cluster tendency to the mean speed in the Mohosin More intersection. But the maximum vehicle speed was very close to the mean value. However, the frequency decreases if the speed deviates from the mean speed value.

The curve indicates that there were a significant amount of vehicles that traveled near the mean speed value though the overall number of vehicles with high speed and low speed were also significant in this intersection.

4.3.2.1 Cumulative distribution curve

Using the Spot speed frequency distribution curve's data the cumulative speed distribution curve has been prepared. From this curve, the 15^{th}, 50^{th}, $85^{th,}$ and 98^{th} percentile speed has been determined that helps to determine those which travel speed is lower than the desired speed and hence they can create extra traffic pressure and delay time as a consequence.

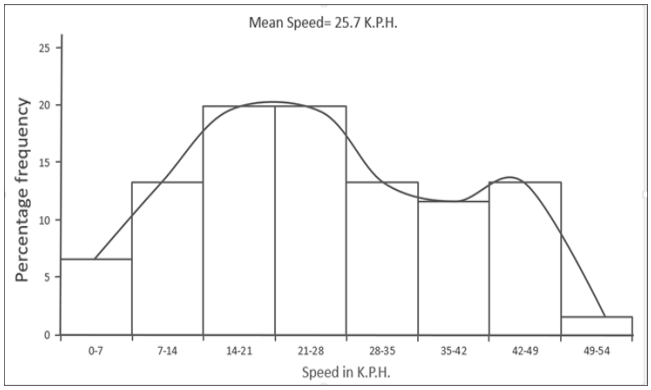

Fig. 10 Spot speed frequency distribution curve for Mohosin More road area.

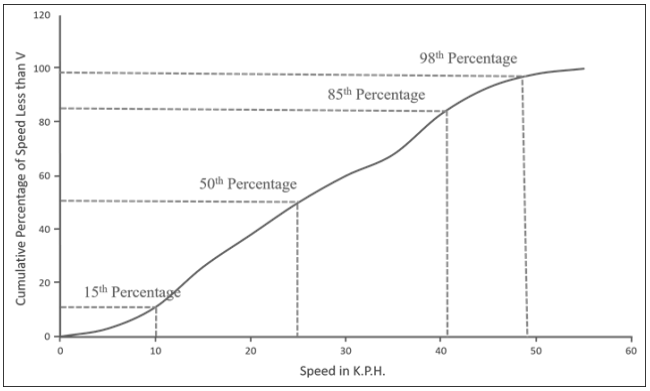

Fig. 11 Cumulative speed distribution curve for Religate intersection road area.

The related percentile speeds for Mohosin More intersection area are as follows:

i. The 15th percentile speed for the Mohosin More road intersection is also 10 K.P.H. which is just similar to the Relegate intersection area. That means 15% of the total vehicles travel equal to or lower than this speed. This speed limit should be prohibited in this section too as this speed limit increases delay time, congestion time, and overtaking tendency to the other drivers.
ii. The 50th percentile speed for this section is 24.5 K.P.H. That means 50% of vehicles travel faster than this speed and the rest of the 50% travels slower than this speed limit.
iii. The 85th percentile speed for this road section is 41.38 K.P.H. That means in a free-flowing condition 85% of all vehicle travel within this speed limit. Normally this speed limit is considered as the maximum allowable safe speed for any road.
iv. The 98th percentile speed for Mohosin More Road area is 48.75 K.P.H. This speed can be considered as the design speed for this road.

Table 4 reveals that Mahindra and Easy bike have the highest coefficient of variation with a maximum speed of 29.50 K.P.H and 24.29 K.P.H. respectively. It means that they could move faster if they don't face any congestion. Mahindra and Easy bike account for a very large portion of traffic composition on the road. The minimum speed of Mahindra and Easy bike go much lower than the 15th percentile speed for this section. It means that if queuing is formed during congestion, this traffic mode makes the congestion more acute as other vehicles need to overtake opportunities while approaching to move.

The direct field survey data (Fig. 12) also approves the results of Table 4. Just like the Religate intersection, in the Mohosin More intersection, the minimum spot speed of Easy bike and Mahindra found lower than the 15th percentile with a speed of only 5 K.P.H and 4 K.P.H respectively. According to the field survey data, Easy bike and Mahindra tends to stop in these intersections to collect passenger which creates unwanted queue in this study area. This consequently adds extra traffic pressure and travel time delay as result.

Table 4 Spot speed statistics of different types of vehicles on Mohosin More intersection.

Vehicle type	Speed of Vehicles				
	Mean	Maximum	Minimum	Standard Deviation	Coefficient of variations
Easy bike	13.32	24.20	5.00	6.09	0.46
Mahindra	17.45	29.50	4.00	9.13	0.52
Motorcycle	31.31	53.25	15.50	12.81	0.41
Private Car	34.77	48.75	16.20	10.63	0.31
Bus	30.57	43.20	12.25	9.24	0.30
Truck	26.76	42.75	12.50	10.16	0.38

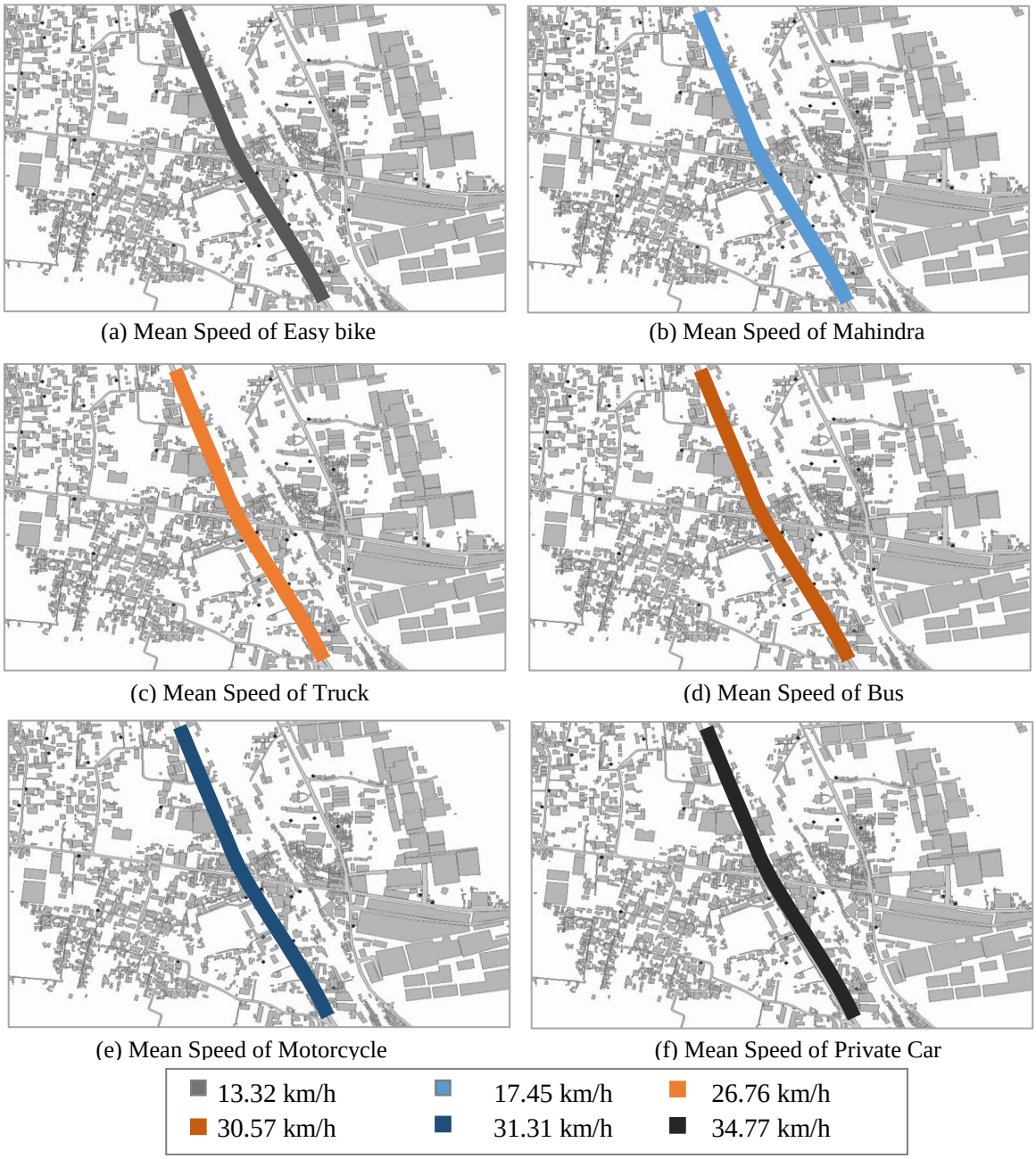

Fig. 12 Mean speed map for different vehicles in the Mohosin More intersection.

5. Conclusion

A comparison among travel time, running time, delay in peak, and off-peak hours on different days of a week is out in this study. From the result and analysis conclusion has been made that workdays have high travel time & delay compared to the weekends. The study shows the relation between traffic flow and delay time, as the traffic flow increases the delay time also increases. On the other hand, the reasons behind the delay time are also found out in Religate and Mohosin More intersections. Vehicles with less than or equal 10 K.P.H. are responsible for increasing the delay time and congestion significantly in these intersections, as it is the 15th percentile speed for these intersections. Easy bike and Mahindra have a minimum speed of 5 K.P.H and 4 K.P.H respectively at Mohosin More intersection and for Religate intersection the minimum spot speed of Easy and Mahindra are 4 K.P.H and 5.75 K.P.H respectively. As the minimum speed of Mahindra and Easy bike are much lower than the 15th percentile speed for these sections, they are responsible for increasing the delay time and congestion significantly on this road.

References

[1] Hossain, M.A. and Imam, M.O., 2018. Traffic Congestion Monitoring in The Selected Transport Axis of Chittagong City. *International Conference on Advances in Civil Engineering*, 1-2.

[2] Forde, A. and Daniel, J., 2020. Pedestrian walking speed at un-signalized midblock crosswalk and its impact on urban street segment performance. *Journal of Traffic and Transportation Engineering (English Edition)*.

[3] Islam, M., Ali, R.B., Chowdhury, F.K. and Sobhan, M., 2019. Road Accident Analysis and Prevention Measures

of Rajshahi-Sirajganj Highway in Bangladesh. *World Scientific News*, *126*, pp.209-221.

[4] Dowling, R.G. and Reinke, D., 2008. *Multimodal level of service analysis for urban streets* (Vol. 128). Transportation Research Board.

[5] Jahan, S., Sustainable and inclusive transport development in Bangladesh. Bangladesh University of Engineering and Technology.

[6] Chakrabartty, A. and Gupta, S., 2015. Estimation of congestion cost in the city of Kolkata—A case study. *Current Urban Studies*, *3*(02), p.95.

[7] Tasnim, S. and Khan, M.M.H., Impact of physical feature on traffic congestion: a case study of khulna jessore highway, khulna. *International Conference on Civil Engineering for Sustainable Development*.

[8] Najneen, F., Hoque, K.S., Mahmood, S.M.S., Rahman, S. and Sharmin, M., 2010. Traffic congestion due to unplanned activities on road-A case study on Gollamari-Satkhira, outer by-pass (Phase-II) and Gollamari-Batiaghata Road. *Bangladesh research publications Journal*, *4*(2), pp.185-197.

[9] Mahmud, K., Gope, K. and Chowdhury, S.M.R., 2012. Possible causes & solutions of traffic jam and their impact on the economy of Dhaka City. *J. Mgmt. & Sustainability*, *2*, p.112.

[10] Moniruzzaman, M., 2013. Sustainable and inclusive transport development of Khulna City. *Khulna: Khulna City Corporation*, pp.1-27.

[11] Akmal, A., & T., K., 2015. The Impact of Speed Radars on Drivers Behavior: A Case Study in Dubai. International *Journal of Traffic and Transportation Engineering*, 4(5), 123-130.

[12] Haque, M.N., Farhan, H.M., FarhanaSultana, A.H., Jahan, J., Rahman, M.M. and Das, P.C., 2018. Evaluating operational characteristics of public transport system of khulna-jessore highway, bangladesh: a case study on phultala to afil gate mid-block. *International Conference on Civil Engineering for Sustainable Development*.

[13] Faghri, A. and Hamad, K., 2002. Travel time, speed, and delay analysis using an integrated GIS/GPS system. *Canadian Journal of Civil Engineering*, *29*(2), pp.325-328.

[14] Shatnawi, I., Yi, P. and Khliefat, I., 2018. Automated intersection delay estimation using the input–output principle and turning movement data. *International Journal of Transportation Science and Technology*, *7*(2), pp.137-150.

[15] Saha, A.K., BA, M.R. and Nahar, T.T., 2013. Analysis of Traffic Congestion and Remedial Measures at Traffic Mor i n Pabna City. *Bangladesh International Journal of Recent Development in Engineering and Technology*, 1(2), pp.23-26.

[16] Mondal, S. and Hossain, Q.S., 2016. Assessing the level of traffic congestion at ferighat intersection in khulna metropolitan city. *International Conference on Civil Engineering for Sustainable Development*.

[17] Department, R. A., 2009. Road Master Plan. Roads and Highways Department.

[18] Mathew, T. V., 2019. Moving observer method. *Transportation Systems Engineering*.

[19] Hou, Y., Sun, C. and Edara, P., 2012. Statistical test for 85th and 15th percentile speeds with asymptotic distribution of sample quantiles. *Transportation research record*, *2279*(1), pp.47-53.

[20] Yang, J., Xu, J., Gao, C., Bai, G., Xie, L. and Li, M., 2019. Modeling of the Relationship Between Speed Limit and Characteristic Speed of Expressway Traffic Flow. *Sustainability*, 11(17), p.4621.

[21] Khan, J.A. and Tarry, S.R., 2018. Speed spot study by comparing time mean speed and space mean speed: A case study. *International Journal of Advanced Science and Research*, 3(1), pp.97-102.

SciEn
Journal of Engineering Advancements Vol. 01(03) 2020, pp 85-93 https://doi.org/10.38032/jea.2020.03.003

A Numerical Approach to Investigate the Influence of Resonator Setting and Volume Fraction on Stop Bands in an Acoustic Metamaterial

Riaz Ahmed[1,*], *Hossain Ahmed*[2] *and Sourav Banerjee*[2]

[1]University of Wisconsin - Green Bay, Green Bay, WI 54311, USA
[2]University of South Carolina, Columbia, SC 29208, USA

Received: September 23, 2020, Revised: September 28, 2020, Accepted: September 29, 2020, Available Online: October 03, 2020

ABSTRACT

A quest for physics-based understanding of engineered metamaterials inspired numerous researchers to extract intricate features such as guiding and filtering elastic waves, wave focusing, topological insulation, cloaking etc. A traditional metamaterial is composed of a heavy core along with some other materials of dissimilar mechanical properties (e.g. stiffness, density). It is well-established that the frequency band gap can be formed by introducing the desired inconsistency of material properties between stiffer resonators and adjacent embedding matrices. Frequency band gaps are fundamental requirements of many engineering applications such as vibration control, noise mitigation, and energy concentrations. Hence, advanced researches are being carried out continuously to understand the control parameters (e.g. bandwidth, starting and ending frequencies) of the frequency band gap. In this article, a mass-in-mass metamaterial using elliptical anisotropic resonators are considered to investigate the influence of resonators' geometric factors and volume fraction on band gap parameters. While the elliptical resonator is splitted diagonally in one or both opposite ends to analyze the influence of volume fraction of the resonators on stop bands, a second set of half-circular resonators are also investigated to analyze the impact of resonator parameters on frequency bands.

Keywords: Acoustic metamaterial; Band gap; Split-ring resonator; Volume fraction; Wave filtration.

1. Introduction

From the last couple of decades, electromagnetic metamaterials [1],[2] are in concentration to phononic researchers to explore photonic band gaps, a range of frequency where electromagnetic waves cannot propagate [3]. The concept of electrodynamics metamaterial can be used in designing elastrodynamic metamaterials since the physical understanding of electromagnetic wave propagation in photonic crystals is quite similar to the stress (elastic) wave propagation in phononic crystals [4],[5]. Mass-in-mass systems are frequently proposed under elastodynamic problems to predicatively manipulate the frequency band gaps in metamaterials with engineered volume inclusions [6],[7]. Creating local resonance vibration modes is one of the important features of such acoustic metamaterials. Applications of such acoustic metamaterials have been envisioned for waveguiding, vibration control, sound isolation, sensing, energy harvesting etc. [8]-[12].

Band gap and band structure manipulation are increasingly important in acoustic metamaterials to branch out its applicability. It is well-established that in any metamaterial frequency band gap are results from either local resonance or Bragg scattering. Low-frequency sound can be controlled by introducing locally resonant components into phononic crystals [13]-[17], whereas conventionally high-frequency stop bands can be formed by multiple scattering (Bragg) of the periodic inclusion [18],[19]. In recent years, researchers are attempting to manipulate the ability of the metamaterial by artificially designing the system. It has been proven that the number of stop bands can be increased by adding additional local resonators in the system [20],[21]. Most recently a multi-scale mass-in-mass model (MMM) with split-ring resonators [22] is proposed not only to obtain a wider frequency band but also to obtain multiple band gaps in both sonic and ultrasonic frequency regions. The concept of using split rings in a metamaterial system has primarily emerged in photonics research. Movchan et al. [23] used split-ring resonators to control electromagnetic bands in two-dimensional photonic structures. Many other researchers in photonic domain found split ring useful in manipulating electromagnetic waves for specific purposes.

Inspired from these researches, a symmetric split-ring metamaterial system with multiple resonators is considered herein as the model offers a high level of anisotropy. Note that, anisotropy in a unit cell is one of the key factors of dispersive behavior and band gap formation in a mass-in-mass metamaterial system. Although the size effect of the resonators on the respective band gaps was reported earlier [24], the geometric (shape)/volumetric dependency of the resonators on frequency bands is still to explore. Hence, the primary objective of this study is to investigate the possibility to systematically manipulate the frequency band gap by the alteration of the resonator's geometry or volume fraction. In addition, two different sets of resonators in a unit cell are also investigated to understand the influence of resonator setting on the frequency band gap.

2. Model and Computational Approach

2.1 Model Configurations

Several two-dimensional structures with multiple resonator systems (Ref. Fig. 1) are designed to understand the geometric/volumetric dependency of the local resonators on frequency bands. Initially, the unit cell is composed of a heavy core (R1) of diameter 0.1414 inches embedded in a circular ring

*Corresponding Author Email Address: ahmedm@uwgb.edu

(R2) with an outside diameter of 0.2828 inches. A softer material (M1), say, Rubber, is used to seal the space between the heavy core and the circular ring. A similar mass-in-mass system was also proposed by Huang et al. [21]. However, an elliptical ring (R3) is placed at the center of the unit cell to further enhance the anisotropic property of the system (Fig. 1 (a)). The elliptical ring is rotated at 450 about the center of the unit cell to allow identical wave pathway along both x- and y-directions. A much stiffer epoxy material M2 compared to M1 is considered to fill in the elliptical free space. In order to allow continuous mismatch in material stiffness between components in the system, a polymer material (M3) is considered to complete the outer boundary of the unit cell. The outside dimension of the unit cell is measured as one (1) square inch.

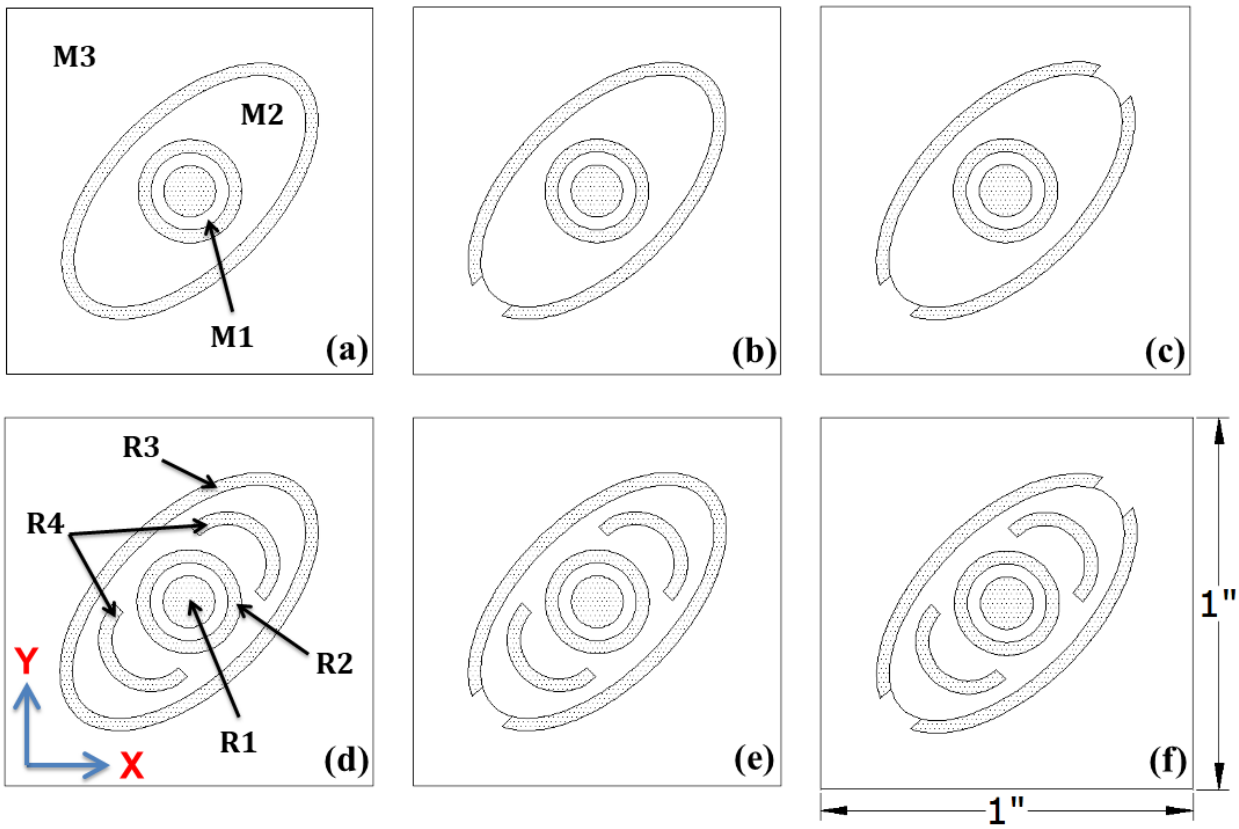

Fig. 1 Projected models to analyze the geometric influence of local resonators on frequency bands. Models (1a-1c) with resonators R1-R3 are considered as set-1 and rest (1d-1f) as set-2 with R1-R4 resonators.

While designing, the elliptical resonator is splitted about 0.115 inches along its major axis in both one (Fig. 1(b)) and two (Fig. 1(c)) directions, respectively. Such splitting of the resonators not only decreases the volume fraction of the resonators in the unit cell but it also allows additional degrees of freedom in the system, which tends to alter the frequency bands. The splitting of the resonators was made at the ends of the major axis of the elliptical geometry to ensure similar wave propagation path along x- and y- directions. In order to analyze the geometric influence of the resonators more rigorously, especially the effect of resonator setting, a pair of half-circular rings (R4) are added symmetrically (Figs. 1(d)-1(e)) in all three models described previously (Figs. 1(a)-1(c)). Unit cells with resonators R1-R3 are considered as resonator set-1 (Models 1a-1c); whereas set-2 is referred to as models with resonators R1-R4 (Models 1d-1f). In this study, the thickness of all the rings is considered as 0.037 inches. Material properties and dimensions of the unit cell components are listed in Table 1.

Table 1 Properties of the components of the unit cell.

Component Name	Outer Dimensions (inch)	Stiffness (Pa)	Density (kg/m^3)	Poisson's Ratio
M1	Diameter – 0.2121	10e6	980	0.49
M2	Major Radius – 0.4 Minor Radius – 0.2	2.5e9	1250	0.38
M3	1 X 1 Square	0.5e9	1050	0.49
R1	Diameter – 0.1414	13e9	11310	0.435
R2, R4	Diameter – 0.2828	100e9	2950	0.31
R3	Major Radius – 0.435 Minor Radius – 0.235	100e9	2950	0.31

2.2 Numerical Simulation

The mathematical formulation of infinitely repeating split ring unit cell proposed in this study requires the implementation of Bloch theorem. Since it is challenging to perform analytical derivation of such a material system, the widely accepted Finite Element Method has been utilized to solve this problem. While calculating the dispersion relation, the complete structure is considered infinite in both x- and y- directions by arranging the unit cells or the Representative Volume Elements (RVEs) periodically. To implement this concept, the Bloch-Floquet periodic boundary condition is applied at all boundaries of the RVE. These boundary conditions are based on the Floquet theory that can be applied to the problem of vibrations with small-amplitude in spatially periodic structures. The theory states that the solution can be sought in the form of a product of two functions. One follows the periodicity of the structure, while the other one follows the periodicity of the excitation. The problem can be solved on a unit cell of periodicity by applying the corresponding periodicity conditions to each of the two components in the product. Generalized wave equation in the composite material can be written as

$$C_{ijkl}(x_m)\left[u_{k,l}(x_m,t)+u_{l,k}(x_m,t)\right]+f_i(x_m)=\rho(x_m)\ddot{u}_i(x_m,t) \quad (1)$$

where the constitutive matrix containing material properties and the density of the system are the functions of space (x_1, x_2). i, j, k, l & m takes values 1, 2 & 3. Standard index notation is used throughout this manuscript. Let the body force $f(x_m)$be constant.

The unit cells are repeated in both directions and the solution can be assumed in terms of Bloch-Floquet solution as discussed in the previous paragraph. Assuming there is no periodicity along x_3 direction & decoupling the phase component, the displacement solution can be viz.

$$u_i(x_m,t)=\sum_{n2}\sum_{n1}A^i{}_{n1n2}\,exp(ik_m x_m)\,. \quad (2)$$
$$exp(iG_m x_m).exp(ik_3 x_3)\,.exp(-i\omega t)$$

Where, k_m is wave number along m-th direction and G_m is a component of the reciprocal lattice vector along m-th direction. Here, m takes values 1 & 2. G_m can be expressed as $G_m = 2\pi n_m/D_m$, where, D_m is the periodicity of the cells in m-th direction. The $A^i{}_{n1n2}$is the amplitude of the wave modes for particle displacement along i and n_1& n_2 are the integer numbers between $-\infty\ to\ +\infty$. After substituting Eq. (2) in Eq. (1) the Bloch equation with the Bloch operator can be obtained as follows

$$\omega^2\rho(x_m)\sum_{n2}\sum_{n1}A^i{}_{n1n2}\,exp\Big(i(k_m+G_m)x_m - \frac{1}{2}C_{ijkl}(x_m)(k_m + G_m)^2\delta_{mj}\Big)\Big[\sum_{n1}\sum_{n2}A^k{}_{n1n2}\,exp(i(k_l+G_l)x_l) + \sum_{n1}\sum_{n1}A^l{}_{n1n2}\,exp(i(k_k+G_k)x_k)\Big]=0 \quad (3)$$

The above equation is a Bloch eigenvalue problem. The Eq. (3) is then multiplied with Bloch operator with Bloch transformed weighting factor and integrated over the whole domain of the body and the equation was transformed to its weak form. Periodic boundary conditions are applied around the unit cell and weak form of Bloch equation is solved only within the irreducible Brillouin Zone. Further number of amplitude in the Eq. (3) is reduced for each wavenumber (k) point. Thus the n_1& n_2 are reduced from infinity and the truncated set of Bloch mode expansions were used in the solution method. A suitable choice of reduced-order basis was made based on the high symmetry points that characterize the periodic lattice. Next, the Finite Element discretization was performed. Triangular isoparametric elements were used in the simulation. Element sizes were determined based on a series of convergence study and the minimum wavelength occurred in the material. The sizes of the elements were kept to a minimum of 1/10 of the corresponding minimum wavelength that occurred in any material type, respectively. The Bloch displacement amplitudes were discretized using isoparametric shape function $(N_i(\boldsymbol{x}))$ suitable for triangular elements for each combination of n_1& n_2 in their truncated series as follows

$$\boldsymbol{A}_{n1n2}=\sum_{i=1}^{3}N_i(\boldsymbol{x})\Lambda_i \quad (4)$$

Applying the discretization equations and periodic boundary conditions the weak form of Bloch equation reduces to an algebraic eigenvalue problem$[\mathbf{K}(k)-\omega^2\mathbf{M}]\tilde{\mathbf{V}}=\mathbf{0}$, where $\tilde{\mathbf{V}}$ is the discrete Bloch amplitude vector which is periodic within the unit cell. The $\mathbf{K}(k)$ and $\mathbf{M}$ are the global stiffness and mass matrices, respectively obtained by integrating the element level matrices in proper order. Detail expressions for $\mathbf{K}$ and $\mathbf{M}$ can be found in reference. The solution of the eigenvalue problem provided the dispersion curves for the proposed periodic media.

2.3 Validation of Computational Approach

The studied model configurations in this work are quite complex. Hence, it is extremely challenging to perform the mathematical formulation and analytically solve the proposed models. Hence, a simple mass-in-mass system (Ref. Fig. 2) is studied herein using the Finite Element tool to validate the solution methodology.

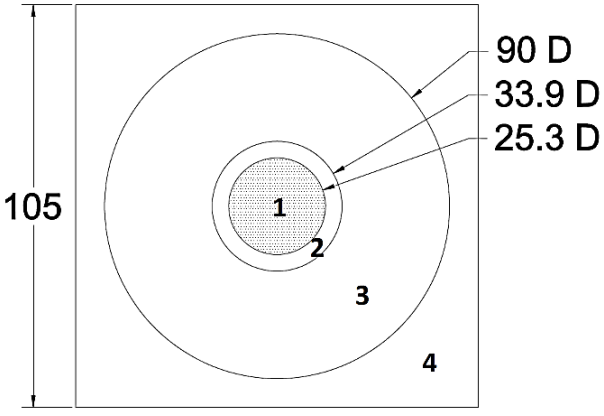

Fig. 2 Single-resonator mass-in-mass system with square periodicity (dimensions are in mm).

In this simple system, a unit cell is designed which is composed of four components. A significantly stiff material, lead (component 1), is chosen as a circular resonator [4],[25]. To avoid evanescent wave modes, the core resonator is coated with softer rubber-like material (component 2). The rubber-lead arrangement is then embedded into a relatively stiffer component (epoxy). The lead-rubber-epoxy combination is synonymous with a well-known mass-in-mass engineered material system proposed by the earlier researchers [20]. It is mathematically proven that such an engineered system provides frequency band gaps (stop bands) by virtually creating negative bulk modulus and negative mass density in the structure [21],[26]. In engineered material systems, the negative responses result from the mismatch of material properties between adjacent components. Hence, to induce further property mismatch, the mass-in-mass system is placed inside a square unit element and the created gap is filled with a relatively softer material (polyethylene plastic).

The complete lead-rubber-epoxy-polyethylene design is considered as the Representative Volume Element (RVE) in this section. The unit cell is a 105 mm square and diameters of the lead, rubber, and epoxy components are considered as 25.4 mm, 33.9 mm, and 90 mm, respectively. The material property of the unit cell components is listed in Table 2.

Table 2 Properties of the components enclosed in the unit cell.

	Lead	Rubber	Epoxy	Polyethylene
Young's Modulus (Pa)	13e9	10e6	3.5e9	0.7e9
Density (kg/m^3)	11310	980	1250	1050
Poisson's Ratio	0.44	0.49	0.38	0.49

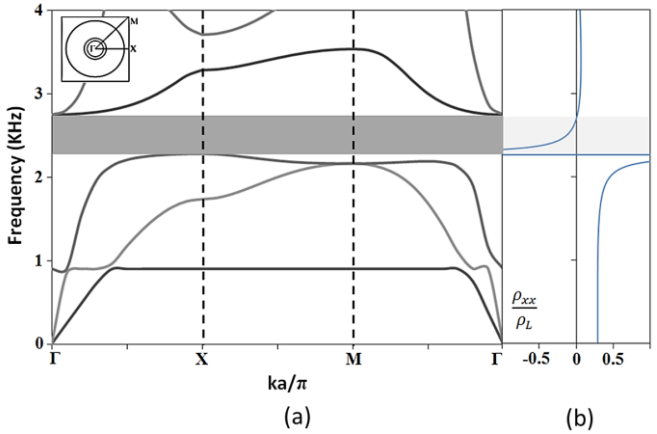

Fig. 3 (a) Dispersion relation (b) Mass density plot for the single-resonator mass-in-mass system.

It is well known that the frequency band gaps are the result of negative mass density and induction of resonance in local microstructures of metamaterials [20],[21],[14],[24]. To validate the above statement and adopted FEM solution methodology, a multi-layered mass-in-mass model (Ref. Fig. 2) is considered. This study is carried out for a frequency range of 0 to10 KHz. For illustration purposes, the response is reported between 0 to 4 KHz in Fig. 3. Computed effective mass densities are normalized by the density of the stiffest component (lead) of the cell. The effective mass density of the unit cell is calculated by Eq. (5) using long wavelength assumption.

$$\rho_{\alpha\beta} = \frac{\int \sigma_{\alpha\beta} d\Gamma}{\int \ddot{u}_{\alpha\beta} d\Gamma} \tag{5}$$

where α, β = 1, 2 and $\sigma_{\alpha\beta}$ and $\ddot{u}_{\alpha\beta}$ are the local stress and acceleration quantities. Γ denotes the external boundary of the unit cell.

The dispersion curve for the single resonator metamaterial within the first Brillouin zone is shown in Fig. 3(a). Using the definition of mass density in Eq. (1), it has been found that the mass density of the system stays negative between the frequency range of 2.27 – 2.71 KHz (Ref. Fig. 3(b)). Alternatively, a stop band is observed (Ref. Fig. 3(a)) at a frequency range between 2.28 - 2.74 kHz (considering Γ-X directional waves). The same band gap continues for the entire Γ-X-M-Γ directional waves. Since the mass density of the metamaterial (calculated using Eq. (1)) is found negative within the frequency range of the stop band, it can be concluded that the analytical and numerical outcomes are in close agreement. This phenomenon is well reported in the literature [20],[21],[14],[24],[27],[28].

3. Results and Discussion

In order to investigate the influence of resonator geometry, six (6) models are proposed as described in Fig. 1. It is hypothesized that resonator geometry as well as the volume fraction of resonators in the unit cell and type of resonator arrangement may have a considerable impact on frequency bands. The dispersion relation of the irreducible Brillouin zone (see Fig. 4(b)) for model 1a (Ref. Fig. 1(a)) is shown in Fig. 4(a). Note that, the wave vector is normalized by the length of the unit cell 'a'.

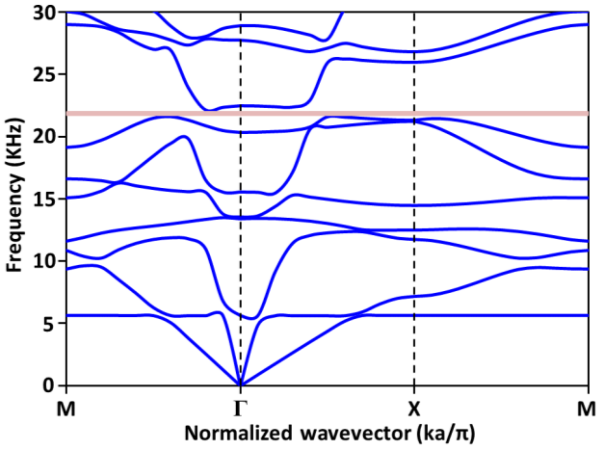

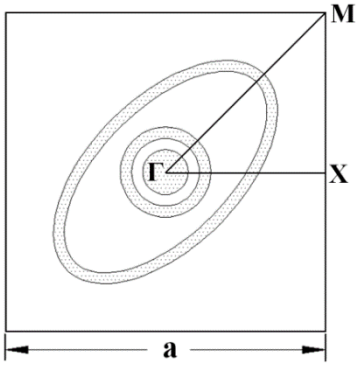

(b)

Fig. 4 (a) Dispersion curve and band gap representation for model 1a. (b) First Brillouin Zone.

In Fig. 4(a), almost all the frequency bands seem highly dispersive, whereas a strong weakly-dispersive (straight) region is observed in the first frequency band, and a stop band is noticed between 7th and 8th frequency bands. The primary focus in this section is to study the transformation of the band gaps due to the alteration of resonator geometry and settings, For comparison, the magnified region of the band gaps for all the models are plotted in Fig. 5 (set 1) and 6 (set 2).

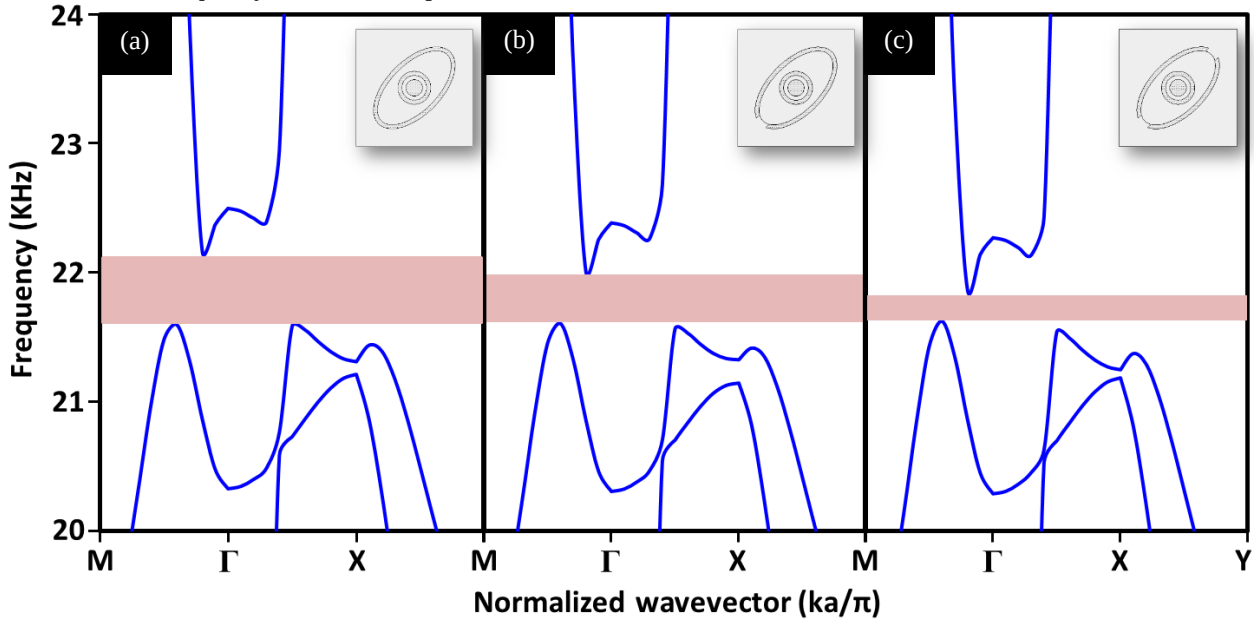

Fig. 5 Magnified dispersion curve representations for resonator set-1 (models 1a-1c).

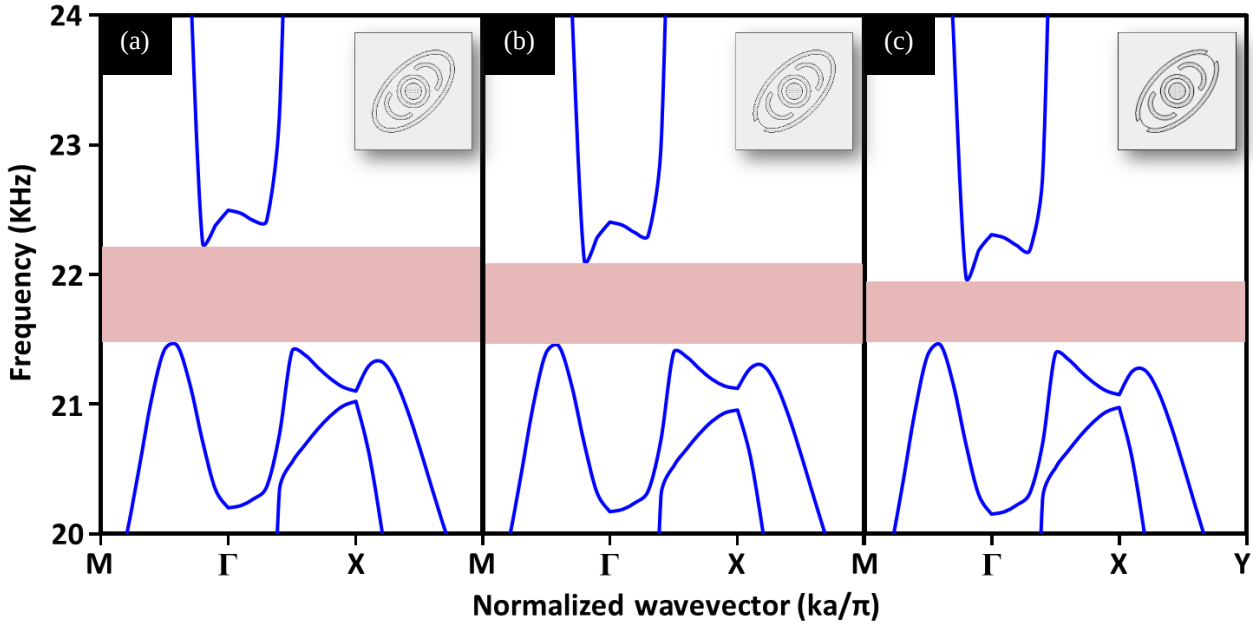

Fig. 6 Magnified dispersion curve representations for resonator set-2 (models 1d-1f).

A band gap with a bandwidth of 562 Hz is observed between 21.598 KHz to 22.16 KHz for the unit cell with a center ball, circular ring, and closed elliptical ring resonators (Fig. 5(a)) and Table 3). However, the bandwidth is reduced to 402 Hz (Fig. 5(b)) and 241 Hz (Fig. 3(c) and Table 3) through the splitting of the elliptical resonator in one end and both ends, respectively. A similar trend is also noticed for other sets of models where two additional half-circular resonators are placed symmetrically. The longest stop band is recorded for model 1d with a bandwidth of 792 Hz and reduced to 661 Hz and 528 Hz, for models 1e and 1f, respectively.

Volume fractions of the resonators in the respective unit cell are listed in Table 3. It is evident that for each set of models, the stop bandwidth can be increased/decreased with the increment/decrement of the volume fraction of the resonators, and it follows a linear pattern. Such a linear pattern is true for any particular set of resonators and can be shifted significantly through the alteration of the resonator set as found in Fig. 7. This finding implies that the same stop band can be maintained with

different volume fractions of the resonators and there is also a possibility to obtain longer band gaps with unchanged volume fraction. In both cases, the selection of resonators configuration in the unit cell would be the key challenge.

Table 3 Obtained band gaps and volume fraction of resonators in the unit cell for studied models.

Model #	Band Start (Hz)	Band End (Hz)	Band Gap (Hz)	Volume Fraction (%)
a	21598	22160	*562*	11.38
b	21608	22010	*402*	11.17
c	21623	21864	*241*	10.96
d	21454	22246	*792*	14.13
e	21453	22114	*661*	13.91
f	21457	21985	*528*	13.70

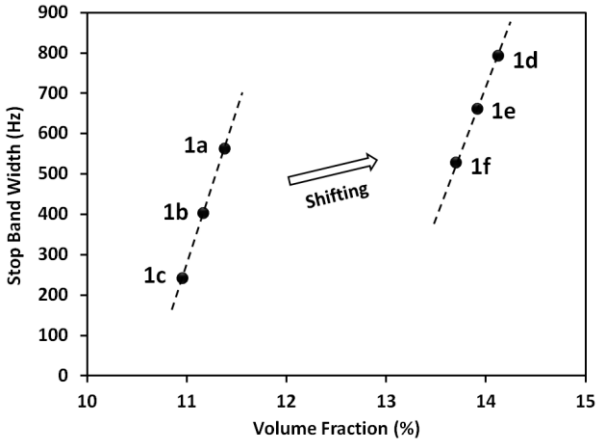

Fig. 7 Stop band manipulation through the alteration of resonators volume fractions and setting in unit cell. Each bullet defines the obtained stop bandwidth with respect to the volume fraction of the resonators in the corresponding proposed model (1a-1f, see Fig. 1).

Fig. 7 shows the influence of the volume fraction of the resonators on OVERALL stop bandwidth. Here, OVERALL means, these stop bands can be found for wave propagation through the model along any direction. While the overall band gap of a structure is important for filtering wave propagation in a three-dimensional space, guided wave propagation (along a specific direction) in a structure is not uncommon. Fig. 8(a) represents the stop bandwidths for both set-1 and set-2 if the wave enters the structure as a guided x-directional (Γ-X) wave. Fig. 8(b) represents a similar phenomenon in the case of the y-directional (X-M) wave. It can be seen that the stop bands are heavily influenced by the volume fraction of the resonator for wave propagation in Γ-X direction, which is similar to the overall response reported in Fig. 7 However, in the case of wave propagation in X-M direction, the effect of volume fraction isn't much significant, where a little increase in stop bandwidth is identified (Fig. 8(b)).

In a bandgap region, it can be seen that two bands from the dispersion curve take a role in forming the stop band (Ref. Fig. 4(a)). To understand the influence of resonator volume fraction on those band gap forming frequency bands, a further investigation is performed and the results are presented in Figs. 9-11. Fig. 9 presents the shift in the lower and upper band of the overall bandgap for different volume fractions. Figs. 10 and 11 present similar outputs for x-directional and y-directional guided waves, respectively. In all these figures, it can be noticed that the volume fraction of the resonators in the unit cell possesses almost no influence on the lower band (start frequency) of the stop band for both sets (a-c and d-f) of models.

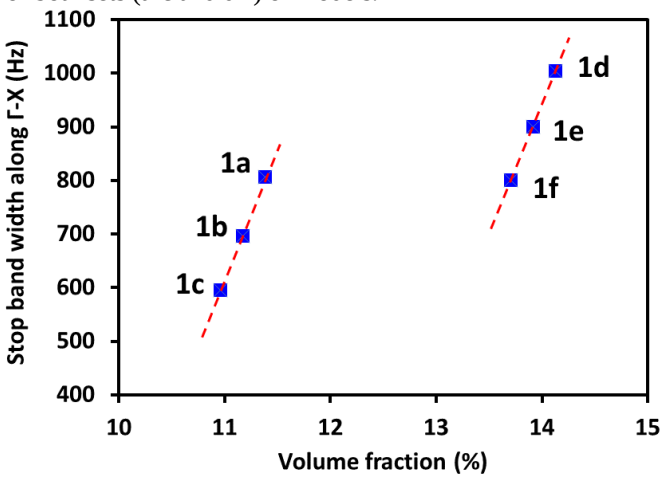

(a)

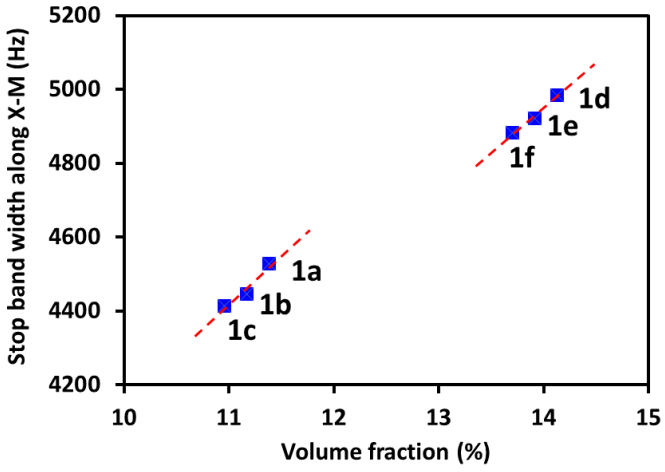

(b)

Fig. 8 Influence of volume fraction on stop bandwidth for wave propagation along (a) Γ-X or x-direction, and (b) X-M or y-direction.

However, the upper bands of the bandgap show a significant dependency on the volume fraction. Note that, for X-M

directional wave incidence (Fig. 11) both the upper and lower band of the band gap show very little reliance on volume fraction. Henceforth, the bandgap width also remains almost unchanged. Upon investigation of the mode shape, it has been found that the frequency bands forming the stop bands along X-M direction are predominantly the result of Bragg scattering, where deformation of the matrix element in the unit cell controls the formation of the band structure. In such instances deformation of the ring resonators is quite negligible. Hence, a change in the volume fraction of the ring resonators making a negligible effect on the band structure or band gap along X-M direction. On the contrary, the upper band to form the frequency band gap along Γ-X direction is the result of the combined effect of Bragg scattering and local resonance of the metal resonators. Such observation is also true for the upper bands of the overall stop bands in Fig. 9. Hence, a change in the volume fraction of the resonators shifted the upper bands for both overall and Γ-X directional waves.

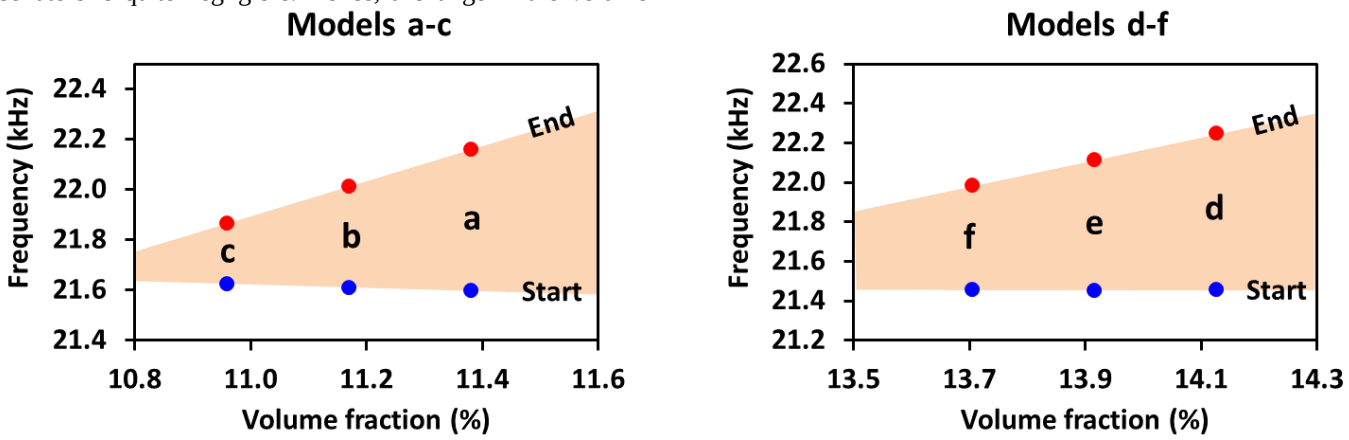

(a) (b)

Fig. 9 Shift in start and end of the overall band gap due to the change in volume fraction

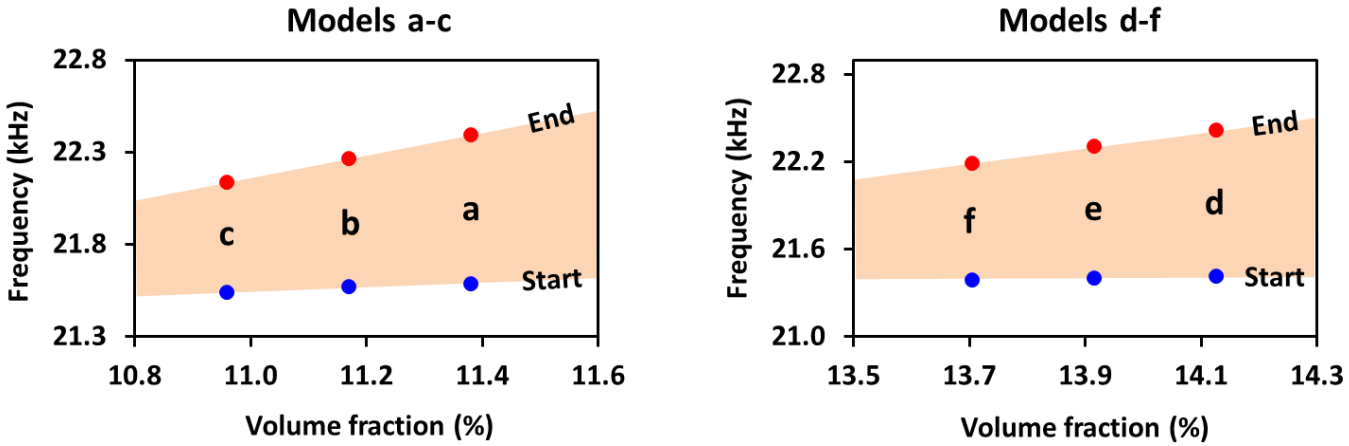

(a) (b)

Fig. 10 Shift in start and end of the band gap along Γ-X due to the change in volume fraction

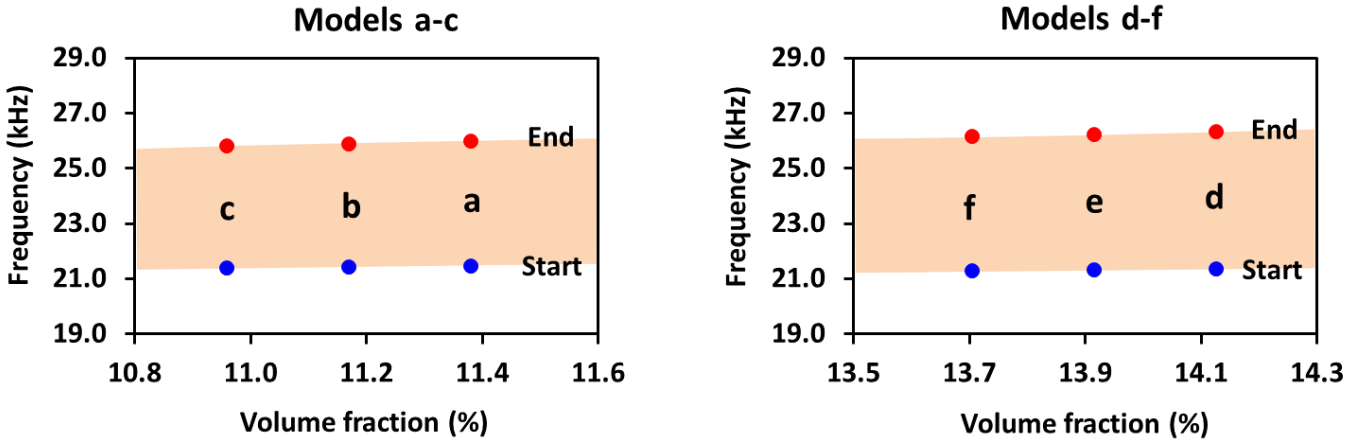

(a) (b)

Fig. 11 Shift in start and end of the bandgap along X-M due to the change in volume fraction

In Figs. 9-11, it can be seen the influence of the resonator's volume fraction on stop bandwidth. However, because of the different scaling in both x- and y-axis it can be a little difficult to identify how much the volume fraction is taking part in controlling the bandgap width for various situations. For example, in Figs. 9-10, all the presentations look almost the same. In that context, the volume fraction possesses almost equal influence for both the set of models and for both overall and x-directional waves. To have a clearer understanding, a percentage increase in bandgap width due to the increase of volume fraction is plotted in Fig. 12. It can be seen that using the model set-1, maximum increase (about 135%) can be obtained in the case of overall bandwidth (ref. Fig. 12(a)). Whereas, almost negligible increase is visible in X-M directional wave. A similar trend can be visible for model set-2 as well (ref. Fig. 12(b)). However, the maximum increase for set-2 in the overall bandgap is about 50%, which is significantly lower than the gain reported for set-1 in Fig. 12(a).

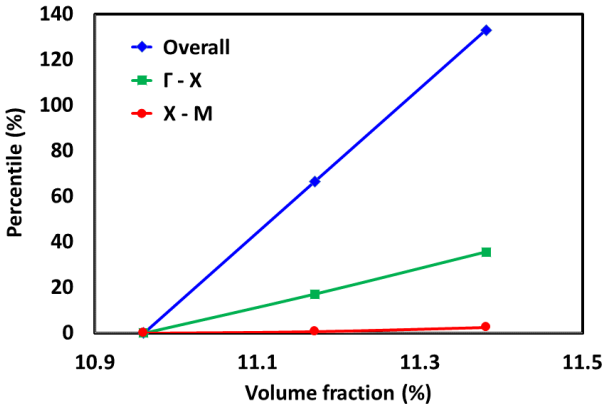

(a)

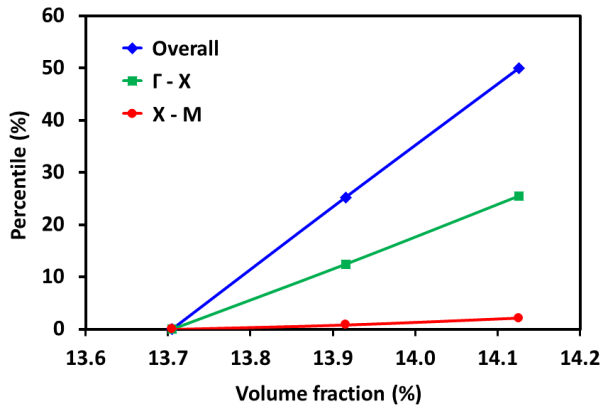

(b)

Fig. 12 Percentage increase in band gap width for models (a) 1a-1c (set 1), (b) 1d-1f (set 2)

4. Conclusion

Manipulating frequency band gaps by designing novel configurations of metamaterials is one of the key areas of interest in recent days. In this purpose, mass-in-mass and layer-in-layer models were proposed by the previous researchers. However, dependency of frequency band gaps on resonator setting and volume fraction of the resonators in a unit cell were still to investigate. In this work, multi-scale mass-in-mass systems containing split-ring resonators are investigated to understand the influence of resonator setting and volume fraction on the frequency stop bands. It has been found that, in any resonating setup, width of the frequency bandgap can be linearly manipulated through the alteration of volume fraction of resonators in the unit cell. However, the linear pattern can be shifted sidewise by changing the resonator set by introducing or taking off a resonator from the unit cell. It has been noticed that lower band of the stop band remains unaffected with the change of volume fraction and the upper band can be shifted upward/downward through the increase/decrease of volume fraction of the resonators. This study also confirms that, with a lower number of resonators it is possible to manipulate the frequency band gap heavily by changing the volume fraction, in comparison to a higher number of resonators. In totality, this study concludes that, in a metamaterial, frequency bands are strongly sensitive to resonator setting and volume fraction in a unit cell.

Acknowledgement

This research was partially funded by the Office of Vice President of Research, University of South Carolina.

References

[1] Smith, D.R., Pendry, J.B. and Wiltshire, M.C., 2004. Metamaterials and negative refractive index. *Science*, 305(5685), pp.788-792.

[2] Pendry, J.B., Holden, A.J., Robbins, D.J. and Stewart, W.J., 1999. Magnetism from conductors and enhanced nonlinear phenomena. *IEEE transactions on microwave theory and techniques*, 47(11), pp.2075-2084.

[3] Smirnova, E.I., Mastovsky, I., Shapiro, M.A., Temkin, R.J., Earley, L.M. and Edwards, R.L., 2005. Fabrication and cold test of photonic band gap resonators and accelerator structures. *Physical Review Special Topics-Accelerators and Beams*, 8(9), p.091302.

[4] Liu, Z., Chan, C.T. and Sheng, P., 2005. Analytic model of phononic crystals with local resonances. *Physical Review B*, 71(1), p.014103.

[5] Mei, J., Liu, Z., Wen, W. and Sheng, P., 2006. Effective mass density of fluid-solid composites. *Physical review letters*, 96(2), p.024301.

[6] Ahmed, R. and Banerjee, S., 2013, April. Novel split ring metamaterial for multiple band gaps and vibration control. In *Health Monitoring of Structural and Biological Systems* 2013 (Vol. 8695, p. 86952L). International Society for Optics and Photonics.

[7] Ahmed, H., Ahmed, R., Indaleeb, M.M. and Banerjee, S., 2018. Multifunction acoustic modulation by a multi-mode acoustic metamaterial architecture. *Journal of Physics Communications*, 2(11), p.115001.

[8] Sigalas, M.M. and Economou, E.N., 1992. Elastic and acoustic wave band structure. *Journal of sound and vibration*, 158(2), pp.377-382.

[9] Poulton, C.G., Movchan, A.B., McPhedran, R.C., Nicorovici, N.A. and Antipov, Y.A., 2000. Eigenvalue problems for doubly periodic elastic structures and phononic band gaps. *Proceedings of the Royal Society of London. Series A: Mathematical, Physical and Engineering Sciences*, 456(2002), pp.2543-2559.

[10] Ahmed, R. and Banerjee, S., 2015. Bio-Inspired Design of a Multi-scale Pass Band Frequency Sensor Using Local Resonance Phenomena. In *Experimental and Applied Mechanics*, Volume 6 (pp. 21-27). Springer, Cham.

[11] Ahmed, R., Madisetti, D. and Banerjee, S., 2017. A sub-wavelength scale acoustoelastic sonic crystal for harvesting energies at very low frequencies (<∼ 1 kHz) using controlled geometric configurations. *Journal of Intelligent Material Systems and Structures*, 28(3), pp.381-391.

[12] Banerjee, S. and Ahmed, R., University of South Carolina, 2020. Power optimization for a unit cell metamaterial energy harvester. *U.S. Patent 10,694,466*.

[13] Hirsekorn, M., Delsanto, P.P., Batra, N.K. and Matic, P., 2004. Modelling and simulation of acoustic wave propagation in locally resonant sonic materials. *Ultrasonics*, 42(1-9), pp.231-235.

[14] Oudich, M., Li, Y., Assouar, B.M. and Hou, Z., 2010. A sonic band gap based on the locally resonant phononic plates with stubs. *New Journal of Physics*, 12(8), p.083049.

[15] Caballero, D., Sánchez-Dehesa, J., Rubio, C., Martinez-Sala, R., Sánchez-Pérez, J.V., Meseguer, F. and Llinares, J., 1999. Large two-dimensional sonic band gaps. *Physical Review E*, 60(6), p.R6316.

[16] Chesnais, C., Boutin, C. and Hans, S., 2012. Effects of the local resonance on the wave propagation in periodic frame structures: Generalized Newtonian mechanics. *The Journal of the Acoustical Society of America*, 132(4), pp.2873-2886.

[17] Ahmed, R.U. and Banerjee, S., 2013. Wave propagation in metamaterial using multiscale resonators by creating local anisotropy. *International Journal of Modern Engineering*, 13(2), p.51.

[18] Liang, X., Wang, T., Jiang, X., Liu, Z., Ruan, Y. and Deng, Y., 2019. A numerical method for flexural vibration band gaps in a phononic crystal beam with locally resonant oscillators. *Crystals*, 9(6), p.293.

[19] J LUO, J., YAO, L., JIANG, G. and WU, F., 2019. A study on the vibration band gap and vibration characteristics of a cylindrical shell phononic crystal. *Journal of Vibration and Shock*, (8), p.20.

[20] Huang, G.L. and Sun, C.T., 2010. Band gaps in a multiresonator acoustic metamaterial. *Journal of Vibration and Acoustics*, 132(3).

[21] Huang, H.H., Sun, C.T. and Huang, G.L., 2009. On the negative effective mass density in acoustic metamaterials. *International Journal of Engineering Science*, 47(4), pp.610-617.

[22] Ahmed, R.U. and Banerjee, S., 2013. Wave propagation in metamaterial using multiscale resonators by creating local anisotropy. *International Journal of Modern Engineering*, 13(2), p.51.

[23] Movchan, A.B. and Guenneau, S., 2004. Split-ring resonators and localized modes. *Physical Review B*, 70(12), p.125116.

[24] Hsu, J.C., 2011. Local resonances-induced low-frequency band gaps in two-dimensional phononic crystal slabs with periodic stepped resonators. *Journal of Physics D: Applied Physics*, 44(5), p.055401.

[25] Liu, Z., Zhang, X., Mao, Y., Zhu, Y.Y., Yang, Z., Chan, C.T. and Sheng, P., 2000. Locally resonant sonic materials. *Science*, 289(5485), pp.1734-1736.

[26] Li, J. and Chan, C.T., 2004. Double-negative acoustic metamaterial. *Physical Review E*, 70(5), p.055602.

[27] Milton, G.W. and Willis, J.R., 2007. On modifications of Newton's second law and linear continuum elastodynamics. *Proceedings of the Royal Society A: Mathematical, Physical and Engineering Sciences*, 463(2079), pp.855-880.

[28] Yao, S., Zhou, X. and Hu, G., 2008. Experimental study on negative effective mass in a 1D mass–spring system. *New Journal of Physics*, 10(4), p.043020.

SciEn
Journal of Engineering Advancements Vol. 01(03) 2020, pp 94-100 https://doi.org/10.38032/jea.2020.03.004

Sustainability Analysis of Different Types of Power Plants Using Multi-Criteria Decision Analysis Methods

Anik Saha Dipto[*], *Md Abdullah Al Bari and Shadman Tahsin Nabil*

Department of Mechanical Engineering, Khulna University of Engineering & Technology, Khulna-9203, BANGLADESH

Received: September 14, 2020, Revised: September 29, 2020, Accepted: September 30, 2020, Available Online: October 03, 2020

ABSTRACT

Power requirements are growing day by day, and more power plants are being constructed all over the world. Now the goal has been to look for more sustainable sources of electricity. Sustainability of power plants is a complicated concept and depends on various criteria and sub-criteria. By evaluating them separately creates a complex problem. For this here Multi-Criteria Decision Analysis (MCDA) methods are used for overall assessment and make a sustainability index for seven mostly used power plants. Consideration is taken to both renewable and non-renewable sources. The goal is divided into three basic criteria (i.e. technology, safety & sustainability, economy) and each criterion is further sub-divided into different sub-criteria. The data is collected from various sources and then analyzed using AHP and PROMETHEE methods. The result indicate renewable sources are typically advantageous over non-renewable sources. In certain cases, nuclear has some benefits over other non-renewable energy sources.

Keywords: Sustainability; Power plants; MCDA; AHP; PROMETHEE.

1. Introduction

Sustainability can be termed as a process that satisfies the present needs of people without hampering the generation process for future generations. The sustainability concept is based on three main pillars: social, economic and environmental. The term sustainability was first brought up by the UNESCO in 1987 as a part of boosting the development process. There are goals and visions for this sustainability which take the society to a brighter future [1].

As the need of electrical power is day by day increasing there should be emphasis given on the power sector. Power plant building without any pre-analysis or pre-planning is pretty much unwise by considering future needs of power. As power can be generated from different sources it is wise to analyze which power source to be chosen for more effective performance of the power plant not just in the present but also in the future. So as for this, the sustainability term comes in work. The sustainability of power plants means selecting the appropriate power plant considering different condition and selecting a power plant for both present and future needs.

In Bangladesh defining and understanding the term sustainability for power plants has become very important nowadays because a rumor has been built up whether the construction of new power plants like Matarbari coal-based power plant, Rampal coal-based power plant, Rooppur nuclear power plant etc. are sustainable or not. And why these fuel sources are being chosen instead of other sources likewise gas, oil, wind, solar, etc. The sustainability index can answer this sort of question about their importance in the present and future periods. As being a developing country Bangladesh should keep eye on the sustainable development of power source as the requirement of power will increase exponentially day by day.

For developing a sustainability index for different types of power plants at first the goal is to define sustainability in terms of parameters which can be measured and expressed by data. To do that sustainability is divided into three main criteria as technology, safety and sustainability, and economy [2]. These three criteria are then subdivided into eleven sub-criteria. Now to make a sustainability index, multi-criteria decision analysis (MCDA) method is used. MCDA is the collection of decision-making methods that helps a decision-maker to select a decision based on different data. The data are collected from trusted sources and after analyzing the data a goal can be achieved. Different types of method can be used in order to complete the final analysis. Different types of MCDA methods are named as AHP, ANP, MAUT, MACBETH, PROMETHEE, ELECTRE, TOPSIS etc. These are the most commonly used methods for multi-criteria decision analysis. The decision-making problems can be of different types like, wise ranking problem, rating problem, case problem, etc. But in this analysis only rating and ranking type analysis is done. So, for this research AHP and PROMETHEE methods are selected to carry out sustainability analysis for different types of power plants.

2. Methodology

2.1 Multi-criteria decision analysis

MCDA methods are designed in such a way that it helps people deciding of complex problems which have many alternatives way of solving. When subjective information are loaded in the MCDA system it uses it to solve the problem. The decision-maker is in control of the system and supplies the necessary information to the system. MCDA has a quite large range of applications. Mathematical, social science, informatics, management, marketing, and economics problems can be solved by the MCDA method. Four types of problems are solved widely by using the MCDA method. Ranking problems, sorting problems, choice problems, description problems. In this paper we will use the MCDA to solve ranking and choice problems. For solving choice and ranking problems different types of the MCDA method has been designed. Some of them are,

*Corresponding Author Email Address: aniksahadipto@gmail.com

Table 1 Different ranking and choice-making processes of MCDA

Method Name	Full meaning
AHP	Analytic Hierarchy Process
ANP	Analytic Network Process
MAUT	The Multi-Attribute Utility Theory
MACBETH	Measuring Attractiveness Through a Categorical-based Evaluation Technique
PROMETHEE	Preference Ranking organization method for enrichment evaluation

In our evaluation of the sustainability of different types of powerplants, we have used three methods that are AHP, PROMETHEE, and TOPSIS. For these methods, the alternatives are first selected. There are a total of seven alternatives that are, Coal based plant, Nuclear power plant, Oil based power plant, Gas power plant, Solar power plant, Hydro power plant, and Wind power plant. The main goal is to find the most sustainable power plat for electricity generation. This main goal is achieved by defining sustainability into some criteria. Then the criteria are further sub-divided into some specific sub-criteria.

After each criterion has been defined each of them are needed to be analyzed by the presence of proper data and method and thus a final result can be achieved by MCDA method.

The AHP and PROMETHEE both methods are independent of each other. Only one method is enough to get a suitable result, but here to methods are used in order to see how much the result in individual methods vary from one another.

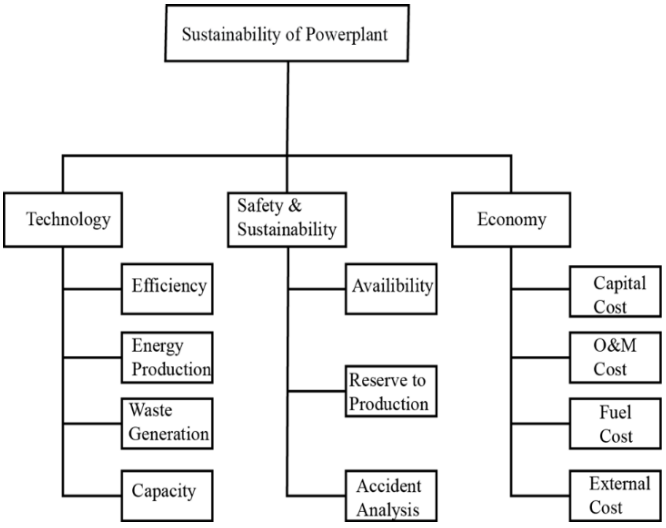

Fig. 1 The analysis of most sustainable powerplant problem by MCDA method

2.1.1 Analytic hierarchy process

AHP is a method that solves a problem by dividing it into some criteria and sub-criteria and analysis it. AHP helps by giving a simple solution to any complex problem. AHP divides a complex problem into simple parts so by solving and analyzing these simple parts together, the whole solution can be acquired. The problems are needed to be structured and these structured problems are needed to compare pairwise for getting a result [3]. A hierarchy is designed to solve the problem. The upper element is the final decision that is to be taken, the second level is the criteria and the criteria is sub divided into some sub-criteria. The sub-criteria can also be sub divided if needed. In our case, we have divided our goal sustainability analysis of power plants into three criteria and eleven sub-criteria.

After the criteria and sub-criteria are designated then the priority of each alternatives is needed to be calculated by a priority matrix. A priority scale has been designated by American School and this is used in AHP method [4].

Table 2 The scale of AHP

Degree of priority	Definition
1	Equal importance
3	Moderate importance
5	Strong importance
7	Very strong importance
9	Extreme importance

The AHP uses the pairwise comparison between the alternatives. The comparison is done manually and then the data is collected in a matrix form. The more the number of alternatives the more effort is needed to be given. If there are n alternatives the number of comparisons for each criterion is $(n^2\text{-}n)/2n^2$, total comparison that is available to a matrix. Each evaluation with alternative with same alternative is regarded as 1. Each alternative is been compared with one another and a comparison matrix is been built. If we take in consideration the technology criteria and efficiency coefficient sub-criteria for AHP analysis first the data is collected, here for sample analysis the efficiency coefficient sub-criterion has been taken into account.

2.1.2 PROMETHEE

The PROMETHEE is also an alternative based choice making method that uses data for analysis and is less manual than AHP. This method has three basic steps:

1. Preference degree calculation for each alternative for each criterion and sub-criterion;
2. The uni-criterion flow analysis;
3. The global flow determination.

For the first step of calculation the data should be unitarized. For this purpose the maximum and minimum value in each data set is to be determined and for beneficial criteria,

$$x_i = \frac{x(i)-min(i)}{max(i)-min(i)}$$

For non-beneficial criterion,

$$x_i = \frac{max(i)-x(i)}{max(i)-min(i)}$$

where,

x_i =Value of any alternative for any sub-criterion

$\max(i)$ =Maximum value of an alternative in that sub-criterion

$\min(i)$ = Minimum value of an alternative in that sub-criterion

Then the values each alternatives value in a criterion should be subtracted with each other to get a value and then the negative value are been neglected. Then each sub-criterion should be divided with its own weight. After that each alternative are summed and value of the global criterion preference matrix is got.

Next, the positive and negative flow is calculated. As it is hard to draw conclusions from preference degrees the criterion preference degree is summarized in a way that is a positive flow or noncriterion leaving and negative flow or noncriterion entering and the net flows are calculated for each alternative. The noncriterion positive flows indicates how an alternative is preferred over all other alternatives. The higher the positive flow is the more preferred the alternative is. On the other hand, the negative flows indicate the average behavior of all alternatives. They show how other alternatives are preferred than this alternative. By considering both positive and negative flow net flow is calculated. The net score lies between -1 to 1. There is two ranking method of PROMETHEE in this study PROMETHEE-II has been used as PROMETHEE-I doesn't give any comparison value [5].

2.1.2.1 The gaia plane

The Gaia plane is an imaginary plane that contains aspects of a decision problem in two dimensional planes. In this Gaia plane, actions are represented by bullets and criteria by arrows. The position of the actions gives the decision-maker some idea about their similarities. The relative position of criterion indicates the correlation and anti-correlation between criterions. The closer are more correlated. The Gaia plane helps decision-maker to visualize conflicting point in the process. The length of the criterion indicates the power of the generated data. So all the information can be got from the Gaia plane in the PROMETHEE method [6].

3. Data

All the data are collected from different free sources available. Here is the data for different sub-criteria:

3.1 Technology

For powerplant technological factors are much important to take into consideration. Technology criterion is sub-divided into four sub-criteria. They are efficiency co-efficient, energy production rate, waste generation and capacity.

Table 3 Efficiency coefficient of 7 types of power plant [7].

Types of powerplant	Efficiency coefficient
Coal	39.4
Nuclear	33.5
Oil	37.5
Gas	43.4
Hydro	80.0
Solar	9.40
Wind	35.0

3.1.1 Efficiency co-efficient

The efficiency coefficient can be defined as the ratio of the energy output to input energy. Efficiency which has relatively high useful energy can be improved by high plant reliability for economic benefit. Understandably, high efficiency is consistent with high plant reliability and low cost of electricity is economically beneficial for powerplant management [8]. As no machine cannot give a unit efficiency, there will be losses in every powerplant. Here presented a statistical analysis done by IAEA 2002 that shows different powerplants efficiency [2]. It shows that hydropower has the most efficiency co-efficient amongst all the sources and solar has the least. Coal has more efficiency co-efficient than nuclear and oil but gas has an upper hand on coal.

3.1.2 Energy production

Energy production rate can be defined as the amount of energy produced by per kg of fuel burning in per hour time. The calorimetric analysis is used to determine the energy production rate of any fuel [9]. A report published by the University of Washington, gives data on energy production of different sources if other factors are constant. It can be seen that gas has the more energy production rate than the other sources and can be more beneficial in selection. Nuclear is more efficient than the other non-renewable and the renewable sources have infinity amount of energy production.

Table 4 Energy production of different power plant [9].

Types of power plant	Energy production (KW.hr/lb)
Coal	4.4
Nuclear	10.6*10^3
Oil	6.67
Gas	19.07
Hydro	Infinity
Solar	Infinity
Wind	Infinity

3.1.3 Waste generation

In this evaluation, the waste generation is taken as the CO2 emission from the different power plants. Measuring the life-cycle greenhouse gas emissions involves measuring the global warming potential of electrical energy sources by assessing the life-cycle of each source. The findings are described in units of potential for global warming per unit of produced electrical energy from that source. Waste generation can be expressed in gram equivalent of CO2 in per KW of energy production. Thomas Bruckner in an article called "Mitigation of Climate Change" published the for CO2 emission from the different power plants [10]. Coal powerplants emit the most amount of carbon-die-oxide and nuclear and wind are the cleanest source of energy.

Table 5 Waste generation from different powerplants [10].

Types of power plant	Waste generation (gCO2eq / kWh)
Coal	820
Nuclear	12
Oil	520
Gas	490
Hydro	24
Solar	48
Wind	12

3.1.4 Capacity factor

The capacity factor is a dimensionless parameter used in the evaluation of power plants. The capacity factor of a powerplant can be defined as the actual amount of energy produced in a certain interval of time and the maximum energy that could have been produced by running the power plant at full power at that time. This parameter or criteria has great importance in power plant evaluation. The capacity generally is less than 100%, as

machines need to do periodic maintenance and sometimes corrective maintenance too. The performance of a power plant greatly depends on its capacity. It is a beneficial criterion. On a report published by EIA, 2019 different powerplant capacity was analyzed [11]. It has been found that nuclear power plant has the height capacity and the solar has the lowest.

Table 6 Capacity factor of different power plant [11].

Types of power plant	Capacity factor
Coal	85
Nuclear	90
Oil	30
Gas	87
Hydro	50
Solar	20
Wind	38

3.2 Safety and sustainability

In the evaluation of powerplants, the safety of human life and the plant equipment must be taken into consideration. Also, the sustainability of energy sources should be ensured. The sub-criteria that are been in this criterion is availability, reserve to production ratio and accidental death analysis.

3.2.1 Availability

In the case of powerplant, the availability describes the time period that a power plant is able to generate electricity over a certain period of time. A power plant can be out of service due to maintenance or repair [12] or due to weather conditions like lack of sunlight or wind *etc.* [13]. The equipment quality, maintenance, types of fuel used and how the operation is done in the power plant greatly affects the availability of the power plant. If other factors are equal power plants which run more do have a higher value of availability. IAEA published a report in 2002 [14] that shows availability of various types power plants. Here it can be seen that nuclear has the most availability on the other hand solar has the least once. Oil and gas dominate over coal power plant.

Table 7 Availability of different power plant [14].

Types of power plant	Availability
Coal	85.4
Nuclear	96
Oil	92
Gas	91
Hydro	50
Solar	20
Wind	38

3.2.2 Reserve to production ratio

The reserve to production ratio is the ratio of the currently available amount of fuel to the annual consumption of each non-renewable resources. When considering the fuel sources only well- known sources are taken into account. Different types of models are used in this case. Non-economic extraction of fuel is not considered as available sources. British petroleum publishes a report every year based on reserve to production ratio of every available non-renewable sources. Here from the BP report 2019 [15] all the data has been taken for 7 types of powerplants. Here it can be seen that all renewable sources have the maximum infinity reserve to production, oil has the most minimum resources compare to other. These values represent the current situation but new sources of energy are been discovered always.

Table 8 Rpr for different power plant [15].

Types of power plant	RPR
Coal	164
Nuclear	70
Oil	40.5
Gas	66.7
Hydro	Infinity
Solar	Infinity
Wind	Infinity

3.2.3 Accidental analysis

One of the vital concerns in the power plant is to ensure the safety of the workers and the public. For this, the powerplant with the least amount of accidental deaths is preferable as human life is more superior to power generation. For the accidental analysis purpose, total amounts of deaths are taken into account until now from different power sources in different types of accidents. Organization for economic and co-operation development published a report that shows deaths from different power plants [16] The maximum amount of deaths are caused by coal-based power plant.

Table 9 Accidental deaths from different power plants [13].

Types of power plant	Accidental Death
Coal	36441
Nuclear	31
Oil	20218
Gas	2043
Hydro	29938
Solar	0
Wind	0

3.3 Economy

For business purposes, the economy should be taken into concern for powerplants as the main purpose of a powerplant should produce energy at a lower cost. So for selecting the best powerplant all costs should be taken into account. The costs that are important in the powerplant economy are capital costs, the operation, and management cost, the fuel cost, the external cost, etc.

Table 10 Capital costs of different power plants [17].

Types of power plant	Capital Costs (€/KW)
Coal	3661
Nuclear	6016
Oil	1802
Gas	1079
Hydro	2752
Solar	7191
Wind	5446

3.3.1 Capital cost

The capital cost can be regarded as the summation of land cost, the necessary cost for infrastructure and the necessary equipment costs that are needed to run the power plant. Labor

costs needed to build the powerplant are not included here. EIA published a report in 2019, publishing the total capital cost needed to build the powerplant [17]. It can be seen that coal and nuclear have relatively high capital costs than others. Oil power plants have lowest capital costs among other electricity generation options.

3.3.2 Operations and maintenance cost

Wages of employees, energy funds, the products and service for power plant operation include the O&M cost. Also, the management cost is included in this cost as it is very much necessary for proper maintenance for the prolonged serviceability of the power plant. Also, if any part of the power plant gets deuterated it is needed to be fixed. The operation management cost is divided into two sub categories; fixed O&M cost and variable O&M cost. Fixed operation cost is the cost that is calculated yearly based and has no effect on the amount of energy produced and the variable cost is directly related to the amount of energy produced. The value of O&M cost is got from the IAE report 2019 [17]. The variable O&M cost are zero for renewable sources as while production they don't need extra maintenance.

Table 11 Fixed O&M cost of different power plants [17].

Types of power plant	O&M Cost (€/KWyr)
Coal	4.613
Nuclear	13.83
Oil	4
Gas	1.6
Hydro	4.75
Solar	9.7
Wind	12.5

Table 12 Variable O&M cost of power plants [17].

Types of power plant	O&M Cost (€/KWyr)
Coal	4.48
Nuclear	2.36
Oil	5.67
Gas	2.54
Hydro	1.39
Solar	0
Wind	0

Table 13 Fuel cost of different power plants [14].

Types of power plant	Fuel Cost (€cent/KWyr)
Coal	1.31
Nuclear	0.27
Oil	1.84
Gas	2.34
Hydro	0
Solar	0
Wind	0

3.3.3 Fuel cost

Fuel is something that is burned and produces energy. For power plant economy it is always required the cheapest value fuel. The cheaper the fuel is the more economic benefit the plant has. Fuel releases energy from the chemical reaction and passes this energy to run the turbine and produces electric energy. The discharge is performed in such a controlled way that this energy can utilize to achieve maximum work. IAEA report 2002 gives a basic price value of all fuels [14]. It can be seen that renewable sources have less fuel cost and gas is the most expensive one.

3.3.4 External cost

These costs are categorized with the extra cost of health and the environment. It is not mixed with the cost of the generation of electricity. These external costs are related to the restoration of the negative side effects that happen on human health as well as the ecosystem during the operation power plant. They are calculated on the basis of the life cycle external cost of the powerplant. By report IAEA 2002 an overview data of different powerplants is got [14].

Table 14 External cost of different power plants [14].

Types of power plant	External Cost(€cent/KWyr)
Coal	8.4
Nuclear	0.49
Oil	6.75
Gas	2
Hydro	0.56
Solar	0.24
Wind	0.16

4. Results and discussion

Here in this analysis two cases have been considered. Case 1 Global criterion and sub-criterion mean taking each criterion with equal importance and the relatively analyzing the sub-criterion based on their relative importance. And case 2 means taking all sub criterion as equal. These cases are not constant, they are both independent. This case varies with time, location etc. So as for sample analysis two basic cases have been considered. Either one of the case can give suitable result.

4.1 Analysis conditions and results by AHP

For the analysis purpose different sample condition were taken by varying the weight of criterion. As by multiplying the weight factor with the priority factor the importance of each alternatives can be got. For analysis purpose two conditions are taken for every method.

4.1.1 Case 1(Global sub-criterion)

For this condition technology, safety & sustainability and economy all the criteria have been considered with an equal weight of 33.33%. Next for determining the weight of each sub-criterion pairwise comparison is done. If the economy criterion is taken as an example every sub-criterion is compared with other pairwise and the pairwise value is got.

Table 15 Pairwise comparison of economy criteria

Sub criterion of Economy	Capital cost	Operation & management costs	Fuel costs	External costs
Capital cost	1	5	1	3
Operation & management costs	1⁄5	1	1⁄5	1⁄3
Fuel costs	1	5	1	3
External Costs	1⁄3	3	1⁄3	1

This is how every criterion is analyzed and a global sub-criteria index is got by the process. As the pairwise comparison is easy and no exact data are not needed for determining the weight, this method is vastly used in the process of determining the weights. The global criteria mainly give information about these three equal criteria. A global ranking of 100% of power plant evaluation different weight of sub-criteria is got which is shown on Table 16.

Table 16 Global Criterion and sub-criterion weight

Sustainability of power plant (100%)					
Technology (33.33%)		Safety and sustainability (33.33%)		Economy (33.33%)	
Energy coefficient	2.33%	Availability	4.30%	Capital Costs	12.92%
Waste Generation	17.5%	Reserve to production ratio	24.71%	Operation & Management Costs	2.20%
Energy Production	9.00%	Accidental death analysis	4.30%	Fuel Costs	12.92%
Capacity	4.55%			External Costs	5.91%

By applying global criterion and sub-criterion weight for different powerplants the final results are got by AHP analysis. It can be seen that the wind power plant is more preferable than the other power plants and hydro is also same preferability like wind. Oil is less preferable than the other sources and nuclear has an advantage on coal.

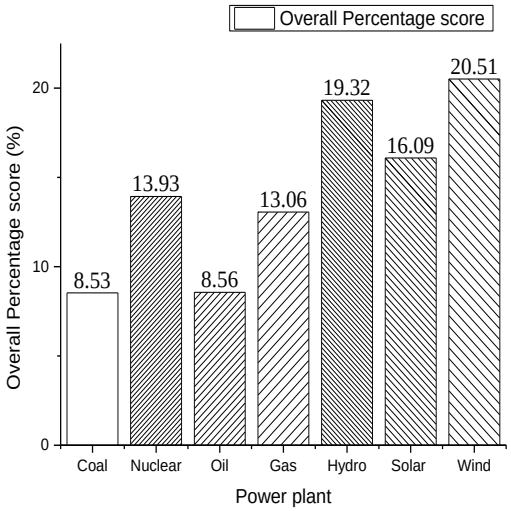

Fig. 2 AHP analysis by Case 1 Global sub-criterion (Equal criteria)

4.1.2 Case 2 (All sub-criteria is of the same weight)

In this case of analysis, all the sub-criteria's weight is regarded as same and they are 9.09% each for every eleven sub-criteria. The result shows that hydro is the most beneficial source if all the sub-criteria are taken as equal and gas has more advantage than other renewable sources like oil, coal

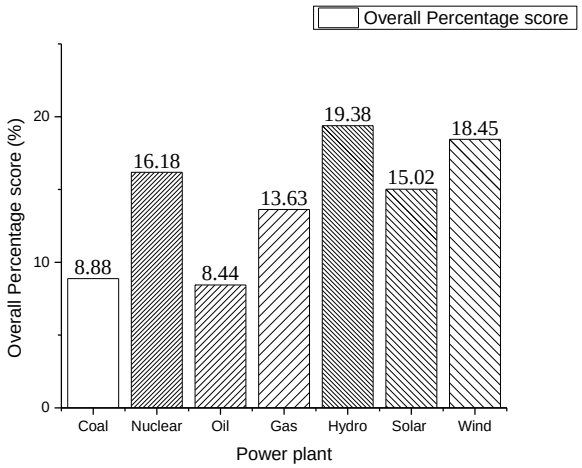

Fig. 3 AHP analysis taking each sub-criterion equal

4.2 Analysis conditions and results by PROMETHEE

In PROMETHEE method the result is shown on the Gaia plane with all scatter points. The higher the position in the y axis the more preferable the power plant is. The Gaia plane is a two-dimensional plane that shows different point in x-y axis with preferable value.

4.2.1 Case 1 (Global sub-criteria weight for every criterion has equal importance)

The value of global flow was determined for global sub-criteria weight by taking each criterion as 33.33%. By the PROMETHEE method analysis, it can be seen that hydropower has the most global flow than other sources. Renewable sources have always the great acceptancy than other sources. Oil has the least amount of acceptancy and nuclear has more acceptancy than coal and oil.

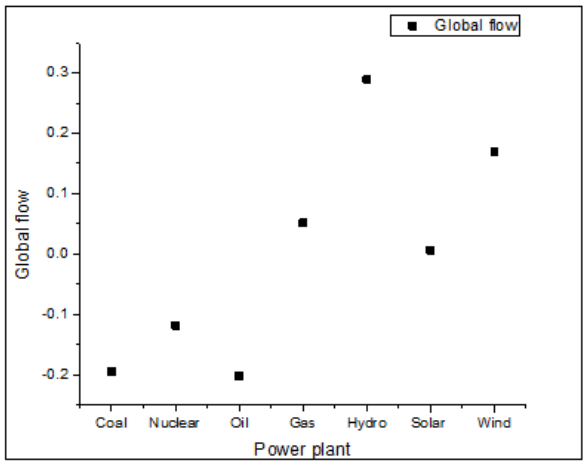

Fig. 3 PROMETHEE analysis by global sub-criteria (Equal criteria)

4.2.2 Case 2 (All sub-criteria is of same weight)

As for this every sub-criterion is 9.09% the global flows show the priority of global flow index for 7 types of power plant. It can be seen that hydro is more efficient than other sources.

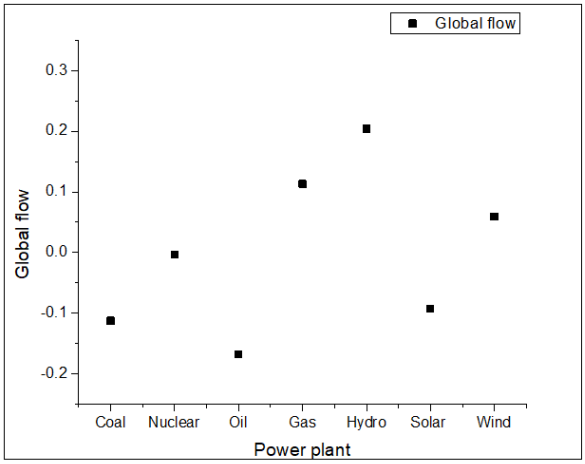

Fig. 4 PROMETHEE analysis taking each sub-criterion equal

4.3 Basic comparison between the AHP and PROMETHEE result

In both AHP and PROMETHEE analysis it has been seen that the renewable sources are better than non-renewable sources and also nuclear has far better sustainability than other sources of non-renewable. From the average result analysis, it can be seen that hydro is the more sustainable source to build and oil is less sustainable source to build. Nuclear power plant plants are much better in case of sustainability.

5. Conclusion

Here the sustainability part was defined properly in the case of power plant and the sustainability of a power plant is divided into some criteria and those-criteria is further sub-divided into several sub-criteria and by this, a hierarchy tree was made. Analytical Hierarchy method and PROMETHEE was studied properly and finally the sustainability index was made. By the analysis of seven types of power plants with respect to technology, economy, and safety & sustainability with the help of the multi-criteria decision analysis for several cases, it can be seen that renewable sources are more sustainable at present. Renewable sources have an endless supply and they can serve as a spontaneous source of energy. Hydro, solar and wind are the highest-ranked power plant in terms of sustainability. The nuclear power plant is also a very beneficial in terms of sustainability and some cases is even more beneficial than renewable sources. Coal has the greatest reserve amongst all the non-renewable fuels analyzed so it can be advantageous too. Gas has an upper hand on coal due to its low capital cost.

References

[1] E. Quality, “What is sustainability?,” 1987.

[2] Pope, J., Annandale, D. and Morrison-Saunders, A., 2004. Conceptualising sustainability assessment. *Environmental Impact Assessment Review*, 24(6), pp.595-616.

[3] Pons, O. and Aguado, A., 2012. Integrated value model for sustainable assessment applied to technologies used to build schools in Catalonia, Spain. *Building and Environment*, 53, pp.49-58.

[4] Olson, D.L., 1997. Decision aids for selection problems. *Journal of the Operational Research Society*, 48(5), pp.541-542.

[5] Brans, J.P. and De Smet, Y., 2016. PROMETHEE methods. In *Multiple Criteria Decision Analysis* (pp. 187-219). Springer, New York, NY.

[6] Ranjan, R., Chatterjee, P. and Chakraborty, S., 2016. Performance evaluation of Indian states in tourism using an integrated PROMETHEE-GAIA approach. *Opsearch*, 53(1), pp.63-84.

[7] Beér, J.M., 2007. High efficiency electric power generation: The environmental role. *Progress in Energy and Combustion Science*, 33(2), pp.107-134.

[8] Chatzimouratidis, A.I. and Pilavachi, P.A., 2009. Technological, economic and sustainability evaluation of power plants using the Analytic Hierarchy Process. *Energy Policy*, 37(3), pp.778-787.

[9] University of Washington, “Energy Content of Fuels,” *Hand Out*, pp. 1–10, 2005.

[10] Schlomer, S., Bruckner, T., Fulton, L., Hertwich, E., McKinnon, A., Perczyk, D., Roy, J., Schaeffer, R., Sims, R., Smith, P. and Wiser, R., 2014. Annex III: Technology-Specific Cost and Performance Parameters, Climate Change 2014: Mitigation of Climate Change. *Contribution of Working Group III to the Fifth Assessment Report of the Intergovernmental Panel on Climate Change*.

[11] EIA, “Electric Power Annual,” *Eia.Doe.Gov*, vol. 0348, no. January, p. 2, 2010.

[12] Ogaji, S.O.T., Sampath, S., Singh, R. and Probert, S.D., 2002. Parameter selection for diagnosing a gas-turbine's performance-deterioration. *Applied Energy*, 73(1), pp.25-46.

[13] Persaud, S., Flynn, D. and Fox, B., 1999. Potential for wind generation on the Guyana coastlands. *Renewable Energy*, 18(2), pp.175-189.

[14] IAEA, “COFACE Annual Report 2002,” no. December, p. 115, 2002.

[15] Spencer, D., 2019. BP Statistical Review of World Energy Statistical Review of World. Ed. *BP Stat. Rev. World Energy*, 68, pp.1-69.

[16] N. Development, Organisation For Economic Co-Operation And Development, no. 6861. 2010.

[17] Cost, E.I.A., 2016. Performance Characteristics of New Generating Technologies. *Annual Energy Outlook*.

SciEn
Journal of Engineering Advancements Vol. 01(03) 2020, pp 100-110 https://doi.org/10.38032/jea.2020.03.005

Combustion and Emission Characteristics of a Diesel Engine Operating with Varying Equivalence Ratio and Compression Ratio - A CFD Simulation

Kazi Mostafijur Rahman and Zobair Ahmed*

Department of Mechanical Engineering, Khulna University of Engineering & Technology, Khulna-9203, BANGLADESH

Received: September 19, 2020, Revised: October 03, 2020, Accepted: October 04, 2020, Available Online: October 05, 2020

ABSTRACT

The performance of diesel engine highly depends on atomization, vaporization and mixing of fuel with air. These factors are strongly influenced by various parameters e.g. injection pressure, injection timing, compression ratio, equivalence ratio, cylinder geometry, in cylinder air motion etc. In this study, a diesel engine has been investigated by employing a commercial CFD software (ANSYS Forte, version 18.1) especially developed for internal combustion engines (ICE) modeling; focusing primarily on the effects of equivalence ratio and compression ratio on combustion and emission characteristics. RNG k-ε model was employed as the turbulence model for analyzing the physical phenomena involved in the change of kinetic energy. In order to reduce the computational cost and time, a sector mesh of 45o angle with periodic boundary conditions applied at the periodic faces of the sector, is considered instead of using the whole engine geometry. Simulations are performed for a range of equivalence ratio varying from 0.6 to 1.2 and for three compression ratios namely, 15:1, 18:1 and 21:1. Results show that, improvement in combustion characteristics with higher compression ratio could be achieved for both lean and rich mixtures. Peak in-cylinder pressure and peak heat release nearer to TDC are achieved for compression ratio of 18:1 that could results in more engine torque. For compression ratio beyond 16:1, effects of fuel concentration on ignition delay is more pronounced. At lower compression ratio, in-cylinder temperature is not sufficiently high for atomization, vaporization, mixing of fuel with air, and preflame reactions to occur immediately after the fuel injection. NOx emission in diesel engine increases due to higher pressure and temperature inside the cylinder associated with relatively higher compression ratio. Rich mixture leads to more CO and unburnt hydrocarbon emission compared to lean mixture as result of incomplete combustion. Engine operation with too high compression ratio is detrimental as emission is a major concern.

Keywords: Computational Fluid Dynamics (CFD), Diesel engine, Compression ratio, Combustion performance, Engine emissions.

1. Introduction

Due to limited reserve of petroleum, ever increasing energy demand and stringent emissions legislation; automakers are striving to develop advanced engine with improved the fuel economy, reduced emissions and higher thermal efficiency. Diesel engine is a high compression ratio internal combustion engine where auto-ignition of fuel occurs due to high temperature developed in the compression stroke. Diesel engine combustion is considered as the series of complex processes and the main events are categorized into ignition delay, uncontrolled rapid combustion phase, mixing controlled combustion phase and after burning phase. The time interval between start of fuel injection and start of combustion refers to ignition delay. This delay period can further be divided into two parts – Physical delay and chemical delay. The fuel, accumulated during physical and chemical delay, is burnt rapidly causing very high heat release in uncontrolled combustion phase. After that the burning rate is controlled by the rate of fuel injection and mixing of fuel with the surrounding air, in controlled combustion phase. After burning phase involves lower rate of heat release due to combustion of remaining fuel [1]. In transportation sector, diesel engine is preferred over petrol engine because of its higher thermal efficiency, better fuel economy and higher engine power and torque. However, they suffer from excessive emissions which require the use of expensive exhaust-gas after-treatment devices [2]. The emission products include soot particles, oxides of nitrogen (NOx), carbon monoxides (CO), unburnt hydrocarbons (UHC) and particulate matters (PM) [3]-[6]. Due to the incomplete combustion of fuel unburnt hydrocarbon (UHC) and carbon monoxides (CO) are generated. The amount of NO_x particles, soot products and other undesired gases in the exhaust gas could be higher than the gasoline engine.

In recent years, extensive researches on diesel engines are ongoing aiming to reduce NOx and soot emission without compromising higher thermal efficiency of the engine. In a study by Reitz et al. [7], the effects of EGR, equivalence ratio and mixing timing on emission levels for heavy duty Premixed Charge Compression Ignition (PCCI) engine has been analysed. At high EGR percentage, drastic reduction in PM levels is reported. Intake temperature is increased with high EGR rate which reduces the PM level. The emissions of PM, NOx and HC are reduced and emission of CO is increased with the increase of mixing timing. As mixing time increases, the charge (fuel-air) becomes more homogeneous and thus reduces emissions. The emission of PM is the function of in-cylinder average equivalence ratio. It is seen that at lean equivalence ratio, PM is not formed. Jindal et al. [8] investigated the effect of compression ratio and injection pressure in a direct injection diesel engine running on jatropha methyl ester. Being a fuel of different origin, the standard design parameters of diesel engine may not be suitable. For small size direct injection constant pressure engine, optimum combination of emission is found at CR 18 with injection pressure of 250 bars. Raheman et al. [9]

*Corresponding Author Email Address: pjk63kj9@s.okayama-u.ac.jp Published by: SciEn Publishing Group

studied the performance of Richardo E6 engine using biodiesel obtained from mahua oil (B100) and its blend with high speed diesel (HSD) at varying compression ratio (CR), injection timing and engine loading. Brake specific fuel consumption (bsfc) and exhaust gas temperature increases, whereas brake thermal efficiency decreases with the increase in proportion of biodiesel in the blends at all compression ratios (18:1 to 20:1) and injection timings (35-45° before TDC). Effect of equivalence ratio on combustion and emissions with a low compression ratio of 14.2 in a dual-fual 6-cylinder engine was investigated experimentally by Jinbao et al. [10]. They reported that the gas consumption rate decreases with the increase of equivalence ratio regardless of strategy in nozzle parameter, exhaust gas recirculation (EGR) rate, injection parameter. Peak heat release rate and exhaust gas temperature increased whereas combustion duration decreased due to the high equivalence ratio in dual fuel ignition mode. Juan et al. [11] studied the knocking tendency in a Cooperative Fuel Research (CFR) engine due to the effect of the varying equivalence ratio. They reported that lean mixture reduces the knocking tendency allowing to operate the CFR engine at higher critical compression ratio. Dong Nam [12] carried out post-graduate research on reducing engine emissions (NOx) from marine diesel engines. He concluded that NOx emission can be reduced by primary methods such as retard injection, fuel nozzle modification, change of compression ratio, water direct injection, water emulsification, exhaust gas recirculation (EGR) and secondary method such as selective catalytic reduction (SCR). Jafarmadar [13] worked on NOx reduction by split injection. In diesel engine, to gain reduction in NOx emission without increasing soot emission is very difficult by adjusting injection timing only. This study demonstrated that split injection could be a promising technique to reduce both NOx and soot emission simultaneously. Recently, numerical simulation of ICE through Computational Fluid Dynamics (CFD) modelling, has become a promising tool to get better insight about the complex processes such as fuel injection, spray formation, chemical kinetics, ignition model, flame propagation, knock phenomena, emission formations that occur inside the cylinder of ICE. Taqizadeh et al. [14] performed numerical investigation of effects of equivalence ratio on combustion characteristics of an RCCI engine. They found that, by increasing equivalence ratio from 0.35 to 0.55 in a constant energy ratio, noticeable growth in the maximum amount of pressure and temperature could be achieved; consequently, NOx emission would increase significantly, IMEP increases by 43%, and ISFC decreases by 30%.

Though many experimental investigations are reported so far, but only a few computational fluid dynamic studies on diesel engines are available in the literature. Therefore, in the present study, effects of equivalence ratio and compression ratio on combustion and emission characteristics in a diesel engine have been investigated through computational fluid dynamics (CFD) modelling.

2. Computational approach

ANSYS FORTE, version 18.1, has been used in this numerical study of diesel engine operating with varying equivalence ratio and compression ratio. This is a fluid-dynamics software that specializes in the simulation of combustion processes in an internal combustion engine, using a highly efficient coupling of detailed chemical kinetics, liquid fuel spray and turbulent gas dynamics. The software solves the full Reynolds-averaged Navier-Stokes (RANS) equations with well-established flow turbulence models. RNG k-ε model was employed as the turbulence model for analyzing the physical phenomena involved in the change of kinetic energy.

2.1 Basic governing equations

The working fluids for internal combustion engines are air-fuel mixture before combustion and the burned products after combustion. Basic fluid dynamics are governed by the Navier-Stokes equation in the turbulent reacting flows. Governing equations are mainly derived by-

- Assuming ideal gas law for gas phase
- The use of Fick's law for mass diffusion
- Assuming Newtonian fluid
- The use of Fourier's law for thermal diffusion

2.1.1 Species conservation equation

$$\frac{\partial \bar{\rho}_k}{\partial t} + \nabla(\bar{\rho}_k \tilde{u}) = \nabla[\bar{\rho}_k D \bar{y}_k] + \nabla\varphi \; + \bar{\rho}_k^c + \bar{\rho}_k^s \quad (Here, k = 1,2,\dots K)$$

Here, ρ is the density, subscript k means species index, K is the total number of species, u is the flow velocity vector

The term φ accounts for the effects for the ensemble-averaging the convection term i.e.

$$\varphi = \bar{\rho}_k \tilde{u} - \overline{\rho_k u}.$$

$\bar{\rho}_k^c$ and $\bar{\rho}_k^s$ are terms due to chemical reactions and spray evaporation, respectively.

2.1.2 Fluid continuity equation

The continuity equation fir the total gas phase fluid is,

$$\frac{\partial \bar{\rho}}{\partial t} + \nabla(\bar{\rho}\tilde{u}) = \overline{\rho^s}$$

2.1.3 Momentum conservation equation

The momentum equation considering the effects of convection, pressure force, viscous stress and turbulent transport as well as the impact from liquid sprays and body force is,

$$\frac{\partial \bar{\rho}\tilde{u}}{\partial t} + \nabla(\bar{\rho}\tilde{u}\tilde{u}) = -\nabla\bar{p} + \nabla\bar{\sigma} - \frac{2}{3}\bar{\rho}\tilde{k}I + \bar{F}^S + \bar{\rho}\bar{g}$$

where, p is the pressure, $\bar{F}^S$ is the the rate of momentum gain per unit volume due to the spray, $\bar{g}$ is the specific body force, $\bar{\sigma}$ is the viscous shear stress, $\bar{\sigma} = \bar{\rho}v\left[\nabla\tilde{u} + (\nabla\tilde{u})^T - \frac{2}{3}(\nabla\tilde{u})I\right]$

V= laminar kinetic velocity, I= identity tensor, superscript T means transpose of a tensor.

The stress accounts for the effects for ensemble averaging of filtering of the nonlinear convection term i.e. $\Gamma = \bar{\rho}(\widetilde{u\tilde{u}} - \tilde{u}\tilde{u})$. In the RANS approach it is called Reynolds Stress.

2.1.4 Energy conservation equation

Based on First Law of Thermodynamics, the change of internal energy has to be balanced by the pressure work and heat transfer. The internal energy transport equation is.

$$\frac{\partial \bar{\rho}\tilde{I}}{\partial t} + \nabla(\bar{\rho}\,\widetilde{u}\tilde{I}) = -\bar{\rho}\nabla\widetilde{u} - \bar{p}\nabla\tilde{u} - \nabla\tilde{J} - \nabla H + \bar{\rho}\tilde{\varepsilon} + \bar{Q}^C + \bar{Q}^S$$

where, I is the specific internal energy, J is the heat flux vector, $\tilde{J} = -\lambda\nabla\tilde{T} - \bar{\rho}D_T\sum_k \bar{h}_k\nabla\left(\frac{\bar{\rho}_k}{\rho}\right)$

λ is the thermal conductivity, which is related to the thermal diffusivity α and heat capacity C_p by $\lambda = \bar{\rho}C_p\alpha$, T is the temperature and $\bar{h}_k$ is the specific enthalpy of species k. $\tilde{\varepsilon}$ is the dissipation rate due to chemical heat release and spray interactions, respectively.

The term H accounts for the effects of ensemble averaging or filtering of the convection term, i.e. $H = \bar{\rho}\left(\widetilde{uI} - \tilde{u}\tilde{I}\right)$

2.1.5 Reynolds averaged navier stokes (RANS) approach

The aim of the RANS is to simulate ensemble-average flow field. The ensemble average is an average that allows the interpretation of the phenomena in terms of the repeatability of multi-component flows.

To model the turbulent transport process gradient-diffusion assumptions are approached. For momentum equation, the deviatoric components of the Reynolds stress are assumed to be proportional to the mean deviatoric rate of strain. The Reynolds stress tensor is,

$$\Gamma = -\bar{\rho}\vartheta_T\left[\nabla\tilde{u}(\nabla\tilde{u})^T - \frac{2}{3}(\nabla\tilde{u})I\right] + \frac{2}{3}\bar{\rho}\tilde{k}I$$

where, ϑ_T is the turbulent kinematic viscosity, if dissipation rate is $\tilde{\varepsilon}$ then,

$$\vartheta_T = C_\mu\frac{\tilde{k}^2}{\tilde{\varepsilon}}$$

$\tilde{k}$ is the turbulent kinetic energy, defined by,

$$\tilde{k} = \frac{1}{2\rho}trace(\Gamma) = \frac{1}{2}\overline{u^{"}u^{"}}$$

C_μ is a model constant that varies in different turbulence model formulations.

The turbulent flux term in the species transport equation is modeled as, $\boldsymbol{\varphi} = \bar{\rho}D_T\nabla\bar{y}_k$, where D_T is the turbulent diffusivity.

Similarly, turbulent flux term

$$H = -\lambda\nabla\bar{T} - \bar{\rho}D_T\sum_k \tilde{h}_k\nabla\bar{y}_k$$

where $\bar{y}_k$ is the turbulent conductivity and is related to the turbulent thermal diffusivity α_T and heat capacity C_p by $\lambda_T = \bar{\rho}C_p\alpha_T$

The turbulent mass and thermal diffusivity are related to the turbulent viscosity by,

$$D_T = \frac{\vartheta_T}{S_{C_T}}$$

$$\alpha_T = \frac{\vartheta_T}{P_{r_T}}$$

where, $S_{C_T}$and P_{r_T} are the turbulent Schmidt and Prandtl numbers, respectively.

2.2 Geometry and mesh generation

In case of diesel engine with equally spaced multi-hole injector, properties such as injection pressure, temperature, air-fuel mixture homogeneity or mixture concentration, combustion process etc. are considered identical with respect to each hole in the injector and the corresponding spray.

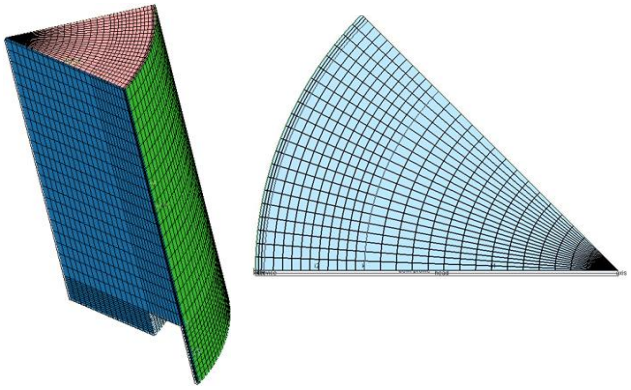

Fig. 1 A 45º sector mesh for modeling diesel engine.

Therefore, the combustion chamber inside the engine cylinder is thought to be symmetrical with respect to each nozzle-hole in the injector. As a consequence, an advantage can be readily obtained by simulating a certain section of geometry instead of considering whole engine geometry for calculation. For example, an eight-hole injector allows simulation using a 45° sector (360°/8). In the current study, for computational domain and mesh generation, a sector of 45° angle with periodic boundary conditions applied at the periodic faces of the sector is considered instead of using the whole geometry of the engine in order to reduce computational cost without comprising the accuracy (Fig. 1).

Table 1 Engine specifications and operating conditions

Engine base type	Cummins N-14, DI diesel
Number of cylinders	1
Cycle	4-stroke
Number of intake valves	2
Number of exhaust valves	1
Combustion chamber	Quiescent, direct injection
Squish	0.56 cm
Bore	13.97cm
Stroke	16.02 (CR=15), 16.21 (CR=18), 16.35 (CR=21)
Range of compression ratio	15:1, 18:1, 21:1
Bowl width x depth	9.79 x 1.55 cm
Connecting rod length	30.2 cm
Engine Speed	1200 rpm
Range of equivalence ratio	0.6 - 1.2
Fuel injector type	Common rail, pilot valve actuated
Number of holes	8, equally spaced
Nozzle orifice area	$3.02\text{x}10^{-4}$ cm^2
Start of Injection (SOI)	-22^0 [After TDC]
Inflow Droplet Temperature	368.0 K
Discharge Coefficient	0.7

A single cylinder DI diesel engine based on a Cummins N-series production engine has been modelled by using ANSYS Forte CFD simulation software. Details of the engine is available in Refs. [15],[16]. The engine specifications and operating conditions are given in Table 1.

2.3 Fuel chemistry and sub-models

For specifying the chemical reaction mechanism for fuel combustion ANSYS Forte supports the industry standard CHEMKIN format. A reduced n-heptane mechanism that can be used to represent the diesel fuel under conventional diesel-engine combustion conditions and available in fuel library of ANSYS Forte is added to the chemistry model in the CFD code to simulate the combustion of diesel fuel. Some other important CFD sub models used in this simulation work are shown in Table 2.

Table 2 CFD Sub-models

Turbulence model	RNG $k-\varepsilon$ model
Droplet breakup model	KH-RT model
Combustion model	Mixing controlled combustion (MCC)
Fuel chemistry model	n-heptane reduced mechanism
Soot model	Two-step semi-empirical model
NOx formation mechanism	Zeldovich mechanism

2.4 Initial and boundary conditions

The initial conditions in the engine simulations are presented in Table 3. These values are utilized for cases with different diesel injection timings and gasoline/diesel ratio. Law of the Wall model is specified for piston, head and liner which can capture wall boundary layer effects more accurately for boundary layers that are thinner than the mesh size. For in-cylinder engine simulations, the turbulent law-of-the-wall velocity condition and fixed temperature walls are usually employed.

Table 3 Initial conditions

Parameters	Value
Intake Valve Closing	165º before TDC
Exhaust Valve Open	125º after TDC
Temperature at Inlet Valve Closing	362 K
Pressure at Inlet Valve Closing	2.215 bar
Turbulent Kinetic Energy	10,000 cm^2/sec^2
Turbulent Length Scale (cm)	1.0
Initial Swirl Ratio	0.5
Initial Swirl Profile Factor	3.11

Table 4 Boundary conditions

Periodicity	45 degree
Wall model	Law of the wall
Piston Temperature	500 K
Head Temperature	470 K
Line Temperature	420 K

3. Results and discussion

3.1 Effect of compression ratio on combustion characteristics:

For diesel engines, the engine combustion is often simulated from intake valve closure (IVC) to exhaust valve opening (EVO), rather than modeling the full air intake or exhaust flow processes involving the intake and exhaust ports, respectively. This is usually a reasonable approximation since the gas in the cylinder at IVC is a relatively homogeneous mixture of air and exhaust gas (due to internal residual or from exhaust-gas recycling), prior to fuel injection. Here, in this study only a part of the engine operation, namely, in between IVC (i.e. 165 degree before TDC) to EVO (i.e. 125 degree after TDC) is simulated for the desired investigations.

Fig. 2 show the combustion characteristics of diesel in terms of in-cylinder pressure, temperature and apparent heat release rate (AHH) for compression ratio of 15, 18 and 21. Both lean mixture with equivalence ratio, ϕ =0.8 and rich mixture with equivalence ratio, ϕ =1.2 are considered to analyse the effect of fuel concentration. It is observed that peak in-cylinder pressure, pressure rise rate, peak in-cylinder temperature, rate of temperature rise and heat release rate, all increase with compression ratio for both lean and rich mixtures. It is well known that, in CI engine prior to fuel injection both air temperature inside the cylinder and cylinder wall (including head, liner and piston top) temperature will be greater for higher compression ratio. This high temperature increases the mixture reactivity, and rate of mixing of fuel with air, causing rapid combustion of fuel that lead to steeper heat release rate, in-cylinder pressure and temperature. Among the three compression ratios, CR=15, CR=18 and CR=21; both peak in-cylinder pressure and peak in heat release are close to TDC for CR=18. It is desirable to have both peak in-cylinder pressure and peak in heat release nearer or closes to TDC as much as possible because these characteristics will lead to maximum engine power or torque. Therefore, it could be concluded that, in terms of combustion characteristics, compression ratio, CR=18 is the optimum one.

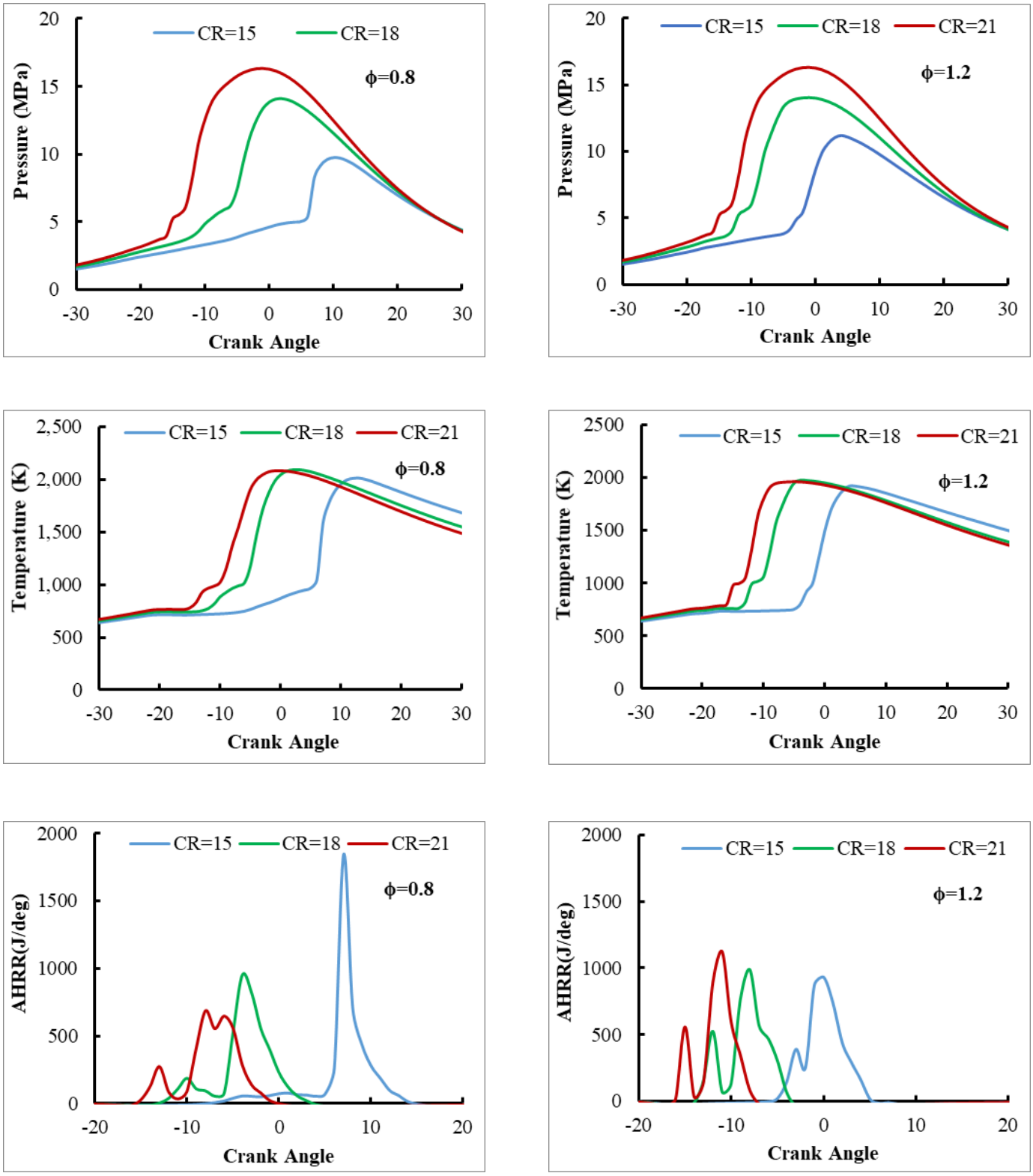

Fig. 2 In-cylinder Pressure, Temperature and Apparent Heat Release Rate (AHRR) Vs Crank angle at different equivalence ratio and compression ratio (for CR=15, CR=18 and CR=21)

After start of injection (SOI) of fuel, the time delay up to start the combustion (SOC) is termed as ignition delay which can be subdivided into physical delay and chemical delay. The higher temperature due to high compression ratio will facilitate atomization, vaporization and mixing of fuel with entraining air inside the combustion chamber, thereby decreasing physical delay. On the other hand, chemical delay also become shorter as high temperature accelerate the pre-flame reactions and make the air-fuel mixture ready for autoignition. Ignition delay becomes shorter with compression ratio over a range of equivalence ratio as depicted in Fig. 3. For compression ratio beyond CR=16, rich mixture shows lower ignition delay compared to lean mixture. At lower compression ratio, for example CR=15, it takes around 17~19 deg. of crank angle (CA) after SOI at 22.5^0 before top dead center, TDC (0^0 crank angle represents TDC). This is because in-cylinder temperature is not sufficiently high for atomization, vaporization, mixing of fuel with air, and preflame reactions to occur immediately after the fuel injection.

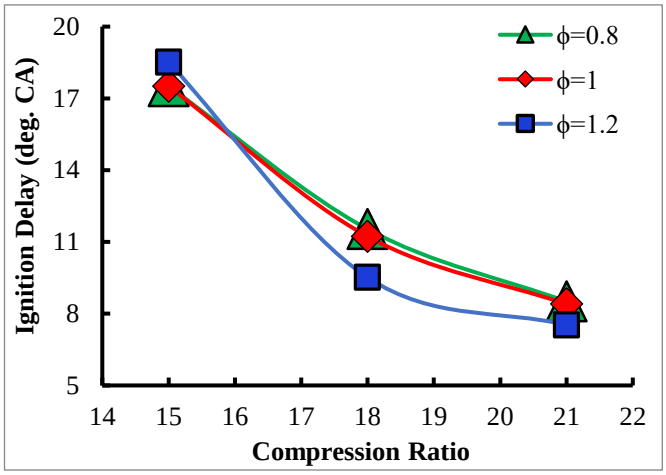

Fig. 3 Ignition delay as function of compression ratio for different equivalence ratios

3.2 Effect of compression ratio on emission characteristics:

It is evident from Fig. 4 that diesel engine NOx emission increases for relatively higher compression ratio. Previously it is seen that higher compression ratio causes higher pressure and temperature inside the cylinder. At high temperature, the nitrogen of the air can react with oxygen and forms various nitrogen oxides e.g. nitric oxide (NO) and nitrogen dioxide (NO2). According to thermal mechanism (commonly known as Zeldovich mechanism) temperature and oxygen concentration are the dominant factors in NOx formation; and it is found to increase exponentially with in-cylinder temperature [1]. This mechanism is highly sensitive to temperature not only because of the high activation energy of reaction but also as a result of the rapidly increasing oxygen atoms concentration in flames with increasing temperature [17]. Fig. 4 clearly demonstrates that for lean mixture with equivalence ratio, ϕ =0.8**,** the exhaust emission of NOx is relatively higher but combustion of rich mixture (ϕ =1.2), reduces NOx emission drastically. As combustion is started earlier with higher compression ratio, therefore, emission of CO is seen to emit earlier in case of CR= 21 and CR=18 compared to CR=15 as shown in the Fig. 4. Besides, introducing relatively higher amount of diesel fuel (ϕ =1.2), results in more CO emission compared to lean mixture with equivalence ratio, ϕ =0.8 which indicates incomplete combustion is more pronounced in case of combustion of rich mixture. Unburnt hydrocarbon emission is observed more in lower compression ratio, CR=15 as a result of poor oxidation associated with lower in-cylinder temperature.

3.3 Effect of equivalence ratio on combustion characteristics:

For diesel engines, fuel concentration plays a vital role on combustion performance in terms of in-cylinder pressure, temperature and apparent heat release rate (AHRR). Fig. 5 illustrates that for fuel rich mixture, combustion of diesel fuel results in faster rate of pressure rise. As more fuel is injected for ϕ =1.0 and 1.2, compared to lean mixture, ϕ =0.6 to 0.8, therefore, a combustible mixture is readily formed in the combustion chamber and autoignition of fuel-air mixture occurs earlier. Though energy supplied is greater for comparatively rich mixture but combustion temperature is found to be lower for ϕ =1.0 and 1.2, compared to lean mixture, ϕ =0.6 to 0.8. This might be attributed to the fact that even after autoignition of fuel-air, the injection of diesel fuel continues to occur directly in burning zone; as a consequence, a portion of the heat of combustion is absorbed by newly injected fuel droplets before vaporization. The highest combustion temperature is observed for ϕ = 0.7 and ϕ = 0.8. In addition, both peak in-cylinder pressure and peak in heat release are close to TDC for ϕ = 0.7 and ϕ = 0.8, which will lead to maximum power or torque.

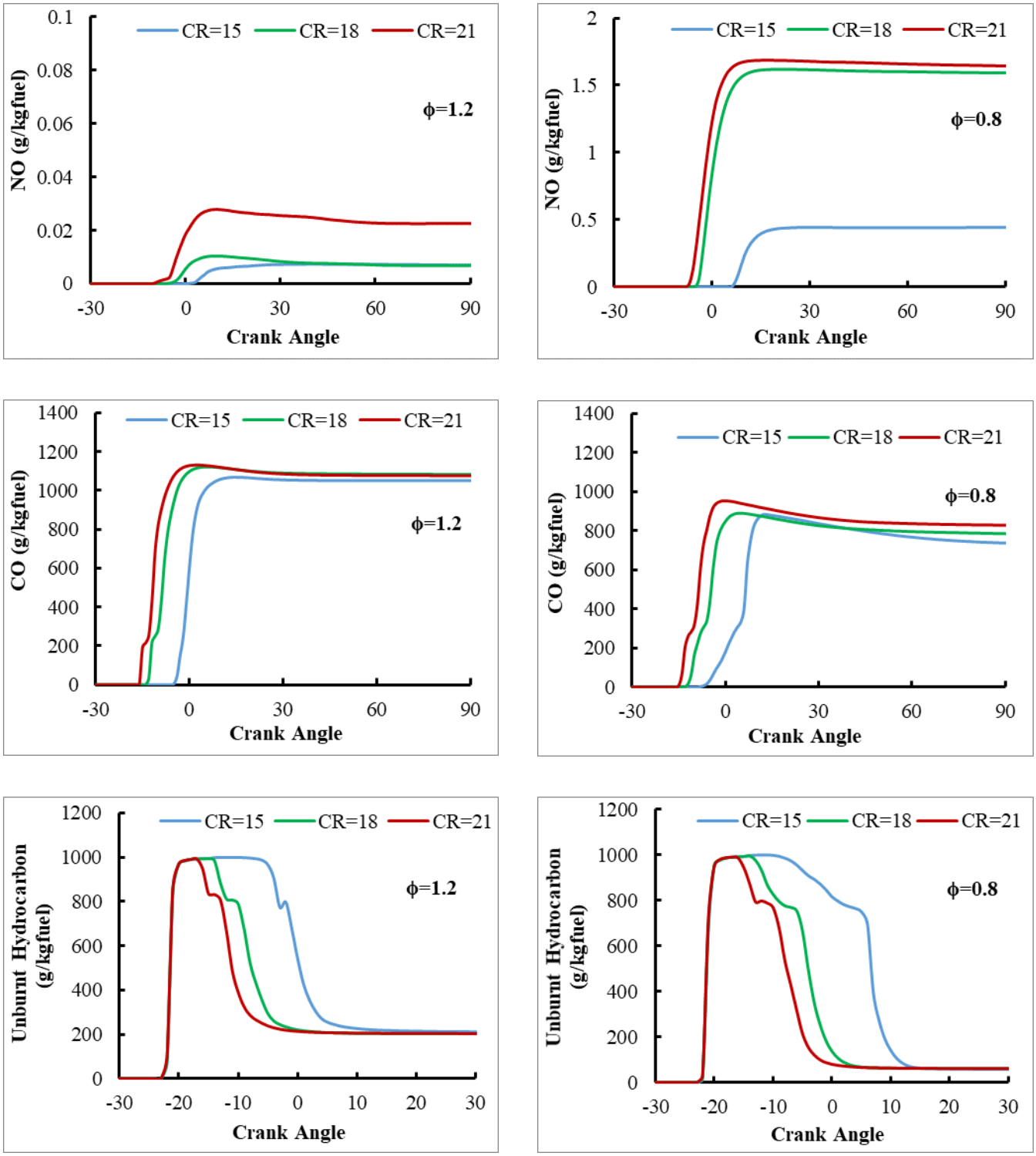

Fig. 4 Emission of NO_x, CO and Unburnt Hydrocarbon Vs Crank angle at different equivalence ratio and compression ratio (for CR=15, CR=18 and CR=21)

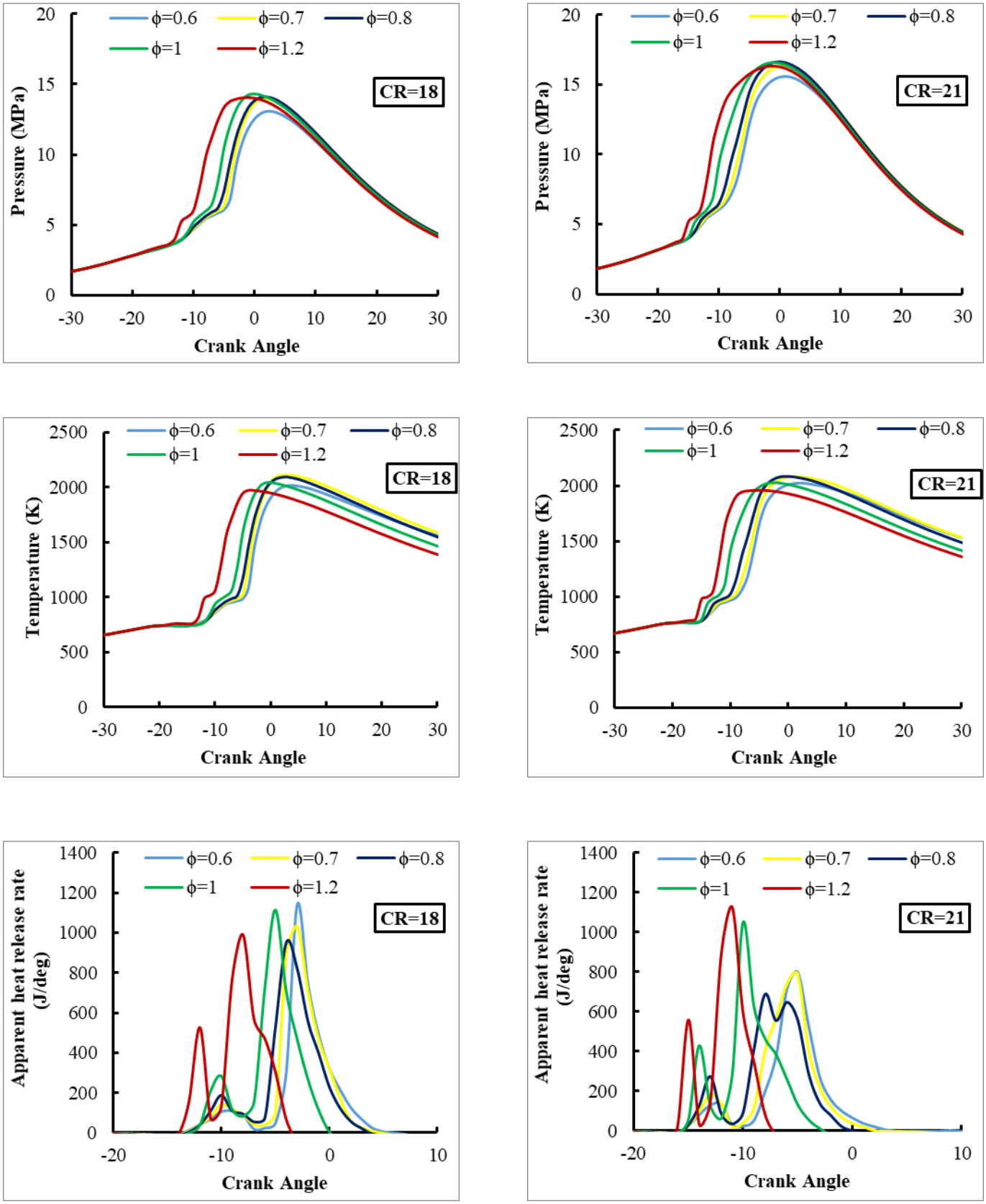

Fig. 5 In-cylinder Pressure, Temperature and Apparent Heat Release Rate (AHRR) Vs Crank angle over a range of equivalence ratio and compression ratio

3.4 Effect of equivalence ratio on emission characteristics:

As mentioned before NOx formation inside the combustion chamber is highly temperature dependent process. It is also well known that lean burn strategy in diesel engine leads to high NOx emission. In the previous section, the in-cylinder temperature is found to be greater for equivalence ratio in the range of ϕ = 0.6 to ϕ =0.8. In this numerical modelling, highest level of NOx emission is observed for lean combustion (ϕ = 0.6 and ϕ = 0.7), as can be seen in Fig. 6. Whereas, for ϕ = 1.0 and ϕ = 1.2, due to low combustion temperature, NOx formation is suppressed significantly. On the other hand, comparative higher compression ratio, CR=21 leads to more NOx emission than that for CR=18.

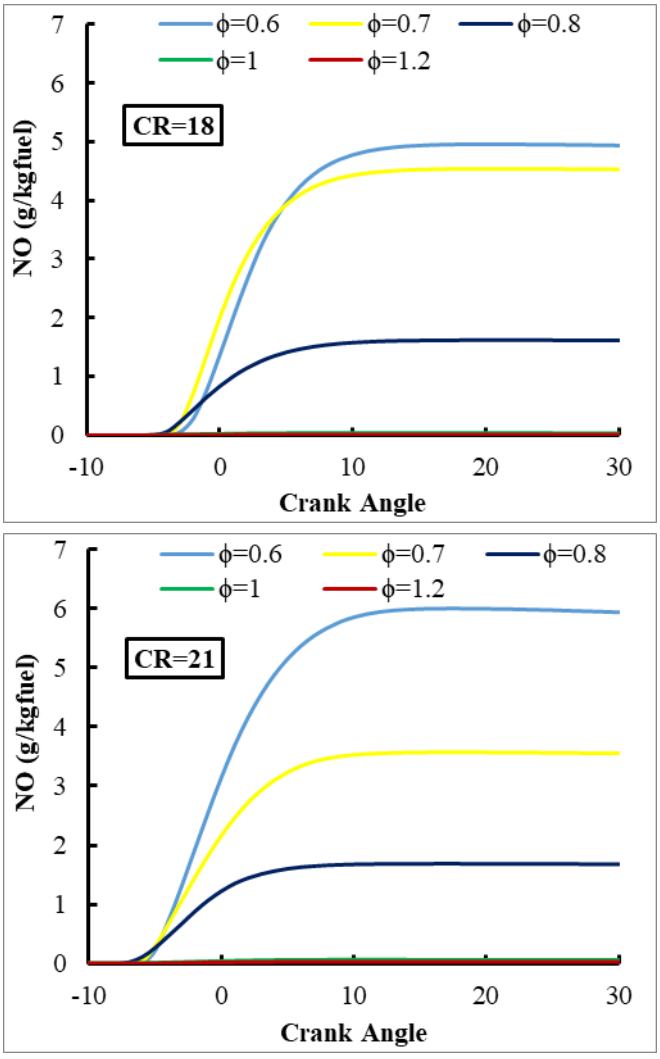

Fig. 6 Emission of NO_x Vs Crank angle for different equivalence ratio and compression ratio

4. Conclusion

In the present study, a diesel engine has been investigated through numerical modelling focusing primarily on the influences of equivalence ratio and compression ratio on combustion and emission characteristics. In order to reduce the computational cost and time, a sector mesh of 45° angle with periodic boundary conditions applied at the periodic faces of the sector, is considered instead of using the whole engine geometry. CFD simulation are performed for a range of equivalence ratio varying from 0.6 to 1.2 and for three compression ratios namely, 15:1, 18:1 and 21:1. For combustion performance, in-cylinder pressure, temperature and apparent heat release rate (AHRR) are analysed whereas emission of NOx, CO and unburnt hydrocarbon are also quantified to highlight the emission performance. Based on the modeling results, the major conclusions that can be drawn are followings:

- Rapid combustion occurs for higher compression ratios and improvement in combustion characteristics with compression ratio for both lean and rich mixtures is observed.
- Peak in-cylinder pressure and peak heat release nearer to TDC are achieved for compression ratio of 18:1 that could results in more engine torque.
- For compression ratio beyond 16:1, rich mixture shows lower ignition delay compared to lean mixture. At lower compression ratio, in-cylinder temperature is not sufficiently high for atomization, vaporization, mixing of fuel with air, and preflame reactions to occur immediately after the fuel injection.
- NOx emission in diesel engine increases due to higher pressure and temperature inside the cylinder associated with relatively higher compression ratio. Rich mixture results in more CO and unburnt hydrocarbon emission compared to lean mixture as result of incomplete combustion.
- For fuel rich engine operation, a combustible mixture is readily formed in the combustion chamber and autoignition of fuel-air mixture occurs earlier.

References

[1] Heywood, J., 1988. Internal combustion engine fundamentals: *McGraw-Hill Education*.

[2] Prasad, R. and Bella, V.R., 2010. A review on diesel soot emission, its effect and control. *Bulletin of Chemical Reaction Engineering & Catalysis*, 5(2), p.69.

[3] Tighe, C.J., Twigg, M.V., Hayhurst, A.N. and Dennis, J.S., 2012. The kinetics of oxidation of diesel soots by NO2. *Combustion and flame*, 159(1), pp.77-90.

[4] Sarvi, A., Lyyränen, J., Jokiniemi, J. and Zevenhoven, R., 2011. Particulate emissions from large-scale medium-speed diesel engines: 1. Particle size distribution. *Fuel processing technology*, 92(10), pp.1855-1861.

[5] Demers, D. and Walters, G., 1999. Guide to exhaust emission control options. *BAeSAME*, Bristol.

[6] Payri, F., Bermúdez, V.R., Tormos, B. and Linares, W.G., 2009. Hydrocarbon emissions speciation in diesel and biodiesel exhausts. *Atmospheric Environment*, 43(6), pp.1273-1279.

[7] Hardy, W.L. and Reitz, R.D., 2006. A study of the effects of high EGR, high equivalence ratio, and mixing time on emissions levels in a heavy-duty diesel engine for PCCI combustion (No. 2006-01-0026). *SAE Technical Paper*.

[8] Jindal, S., Nandwana, B.P., Rathore, N.S. and Vashistha, V., 2010. Experimental investigation of the effect of compression ratio and injection pressure in a direct injection diesel engine running on Jatropha methyl ester. *Applied thermal engineering*, 30(5), pp.442-448.

[9] Raheman, H. and Ghadge, S.V., 2008. Performance of diesel engine with biodiesel at varying compression ratio and ignition timing. *Fuel*, 87(12), pp.2659-2666.

[10] Zheng, J., Wang, J., Zhao, Z., Wang, D. and Huang, Z., 2019. Effect of equivalence ratio on combustion and emissions of a dual-fuel natural gas engine ignited with diesel. *Applied Thermal Engineering*, 146, pp.738-751.

[11] Montoya, J.P.G., Diaz, G.J.A. and Arrieta, A.A.A., 2018. Effect of equivalence ratio on knocking tendency in spark ignition engines fueled with fuel blends of biogas, natural gas, propane and hydrogen. *International journal of hydrogen energy*, 43(51), pp.23041-23049.

[12] Nam, D., 2000. How to reduce emission of nitrogen oxides [NOx] from marine diesel engines in relation to Annex VI of MARPOL 73/78.

[13] Jafarmadar, S., 2013. The Effect of Split Injection on the Combustion and Emissions in DI and IDI Diesel Engines. *Diesel Engine: Combustion, Emissions and Condition Monitoring*, p.1.

[14] Taqizadeh, A., Jahanian, O. and Kani, S.I.P., 2020. Effects of equivalence and fuel ratios on combustion characteristics of an RCCI engine fueled with methane/n-heptane blend. *Journal of Thermal Analysis and Calorimetry*, 139(4), pp.2541-2551.

[15] Dec, J.E., 1997. A conceptual model of DL diesel combustion based on laser-sheet imaging. *SAE transactions*, pp.1319-1348.

[16] Musculus, M.P., 2004. On the correlation between NOx emissions and the diesel premixed burn. *SAE transactions*, pp.631-651.

[17] Anetor, L., Odetunde, C. and Osakue, E.E., 2014. Computational analysis of the extended Zeldovich mechanism. *Arabian journal for science and engineering*, 39(11), pp.8287-8305.

Journal of Engineering Advancements (JEA)

DOI: https://doi.org/10.38032/jea

Indexed by:

Google Scholar

Crossref

Volume 01 Issue 02

DOI: https://doi.org/10.38032/jea.2020.02

Published by: SciEn Publishing Group

Website: www.scienpg.com